buildings

MDPI

Article

Numerical Investigation on the Performance of Exterior Beam–Column Joints Reinforced with Shape Memory Alloys

Mahmoud M. Higazey, Mohammad J. Alshannag * and Ali S. Alqarni

Department of Civil Engineering, King Saud University, Riyadh 11421, Saudi Arabia; mhigazey@gmail.com (M.M.H.); aalqarni@ksu.edu.sa (A.S.A.)
* Correspondence: mjshanag@ksu.edu.sa

Abstract: Upgraded design standards coupled with the damage caused by natural disasters have led to the development of smart materials with the potential to modernize current construction practices. This investigation proposes a nonlinear finite element (FE) model for evaluating the performance of beam–column joints (RC-BCJ) reinforced with shape memory alloys (SMA) and steel rebars. The model was validated based on accredited experimental data, followed by parametric analysis in ABAQUS to optimize the use of SMA bars for enhancing the seismic resistance of RC-BCJ without compromising their energy dissipation capacity. Parameters investigated include the (a) SMA–steel reinforcement ratio, (b) lengths of SMA bars, (c) elastic modulus of SMA, (d) compressive strength of concrete, and (e) axial load applied on the column. The finite element simulation results indicated that the model was capable of predicting the optimum length of SMA bars sufficient for relocating the plastic hinge away from the face of the column along the beam. Further, simulation results proved that the use of SMA bars in conjunction with steel reinforcement could be considered as an effective tool for enhancing the seismic performance of RC-BCJ joints. Among the parameters investigated, high-strength concrete was the most effective in improving joint resistance.

Keywords: reinforced concrete joint; shape memory alloy; energy dissipation; ABAQUS

Citation: Higazey, M.M.; Alshannag, M.J.; Alqarni, A.S. Numerical Investigation on the Performance of Exterior Beam–Column Joints Reinforced with Shape Memory Alloys. *Buildings* **2023**, *13*, 1801. https://doi.org/10.3390/buildings13071801

Academic Editors: Francisco López-Almansa and Roberto Capozucca

Received: 2 May 2023
Revised: 16 June 2023
Accepted: 12 July 2023
Published: 15 July 2023

1. Introduction

In active seismic regions, moderate to severe earthquakes induce permanent inelastic deformation at the beam–column joint interface due to yielding of steel reinforcement at the maximum moment sections. This residual deformation cannot be recovered partially, or fully using the conventional techniques, and design code-recommended practices, respectively. This may lead to poor performance of the structure in terms of ductility and post-yield behavior, losses in serviceability and increased maintenance requirements. After the occurrence of Kobe earthquake in Japan in 1995, there has been an increasing interest in the behavior of beam–column joints subjected to lateral loads. During that earthquake, over 100 reinforced concrete columns with a residual drift ratio of over 1.75% were demolished even though they did not collapse [1]. Residual displacements have been shown to be an important measure of post-earthquake functionality in bridges and buildings and can determine whether the structure remains usable or not [2–5]. Most of the traditional and advanced repair/retrofit techniques used for enhancing the seismic performance of RC-BCJ subjected to cyclic lateral loads were not able to partially or fully recover the residual displacements after unloading. Thus, developing seismic repair and retrofit methods capable of self-centering and displacement recovery is essential for extending the life span and reducing post-maintenance requirements of concrete structures built in active seismic zones. Recently, with the increased awareness of the importance of residual displacements, several novel systems have been investigated to mitigate their effects and improve displacement recovery. A promising new way of resolving this problem is to use smart materials such as SMA in reinforced concrete joints [6–16].

Many theoretical studies have investigated the performance of RC-BCJ using different nonlinear finite element programs. Li and Leong [17] carried out a parametric study through finite element analysis using DIANA [18] for investigating the performance of high-strength interior RC-BCJ. Their test results indicated that the story shears were increased by 12% as the strength of concrete increased from 30 to 40 MPa, and by 15% as the axial load was increased from 0 to 30% of the column axial load capacity. Youssef et al. [19] tested two large-scale RC-BCJ specimens to investigate experimentally the feasibility of using super elastic SMA as a reinforcement for reducing the residual displacements of the joint under cyclic loading. The results demonstrated that SMA RC-BCJ recovered most of its post-yield residual deformation whereas conventional RC-BCJ experienced large residual deformations. The findings of Youssef's study were used by Halahla et al. [20], to determine numerically using ABAQUS [21], the influence of axial load level on the performance of the joint under monotonic load. Their results demonstrated that the presence of axial column load reduces the damage and the cracks in the joints, and allows higher load levels to be applied on the beams prior to failure. Basim et al. [22] carried out a numerical analysis using ABAQUS, on reinforced concrete frames with embedded carbon fiber-reinforced polymer (CFRP) bars in the joints. Their results exhibited a significant increase in lateral load, stiffness and ductility of the joints with embedded CFRP bars. Shannag et al. [23] used nonlinear static (pushover) procedure (NSP) to model and investigate the effect of the fiber content on the performance of interior RC-BCJ using high-strength fiber reinforced concrete in the critical region. They proved that NSP was capable of predicting the load–deflection and moment–curvature of RC-BCJ. Moreover, they discovered that the dissipated energy of RC joints increased significantly with the increase in fiber content. Cao et al. [24] established a 3D model to investigate the dynamic performance of precast prestressed reinforced concrete frames, (RCFs). They emphasized the significance of the slabs on the structural capacity of RCFs in active seismic zones. Moreover, they observed that the variability within the analyzed results is highly dependent on the maximum interstory drift ratio and the residual interstory drift ratio. Oudah and El-Hacha [25] developed single and double slotted beam techniques for self-centering RC concrete connection reinforced with SMA bars. The techniques were experimentally tested under cyclic load and numerically simulated using ABAQUS under monotonic load. Their test results demonstrated that the effectiveness of the system in improving the self-centering capability; reduced the deformations of the joint, and relocated the plastic hinge away from the column face compared to conventional RC-BCJ. Moreover, their results revealed a linear increase in the ultimate load with the increase in concrete strength. In addition, increasing the yield strength of steel from 300 to 500 MPa, resulted in 27.4% in ultimate displacement.

Despite the scarcity of the experimental data available in the literature on the cyclic response of beam–column joints reinforced with SMA bars, which could be due to some practical constraints, in addition to the high cost of SMA. Some researchers [20,26–29], tried to get a deeper understanding of the structural behavior of these joints by carrying out numerical analysis using the finite element software "ABAQUS". However, they reported in their investigations, that the cyclic response of the reinforced concrete beam–column joints could not be addressed adequately using ABAQUS software 2020 because of the pinching effect. Although the self-centering and displacement recovery capabilities of SMA materials are substantial, their lower energy dissipation capacity compared to that of steel is still a controversial issue that limits their use in concrete structures [19,30–33]. This is due to the larger hysteretic loop of steel and the severe cracks concentrated at the plastic hinge area as a result of the inelastic response of structure. Limited or scarce information exist in the literature that addressed the combined effect of SMA bars and steel reinforcement on the structural performance of RC beam–column subassemblages. Therefore, the overall objective of the present investigation was to develop a hybrid system of steel and SMA bars capable of enhancing the structural performance of newly built reinforced concrete beam-column joints. One more objective of this study was to predict the optimum length of SMA bars sufficient for relocating the plastic hinge away from the face of the column along the

beam. The novelty of this investigation relies on taking full advantage of the excellent deformation recovery provided by SMA and the higher energy dissipation capability provided by steel for improving the structural performance of the joint. Moreover, a numerical study using finite element analysis was performed for optimizing the use of SMA bars for enhancing the seismic resistance of RC-BCJ without compromising their energy dissipation capacity. The parameters investigated include the (a) SMA–steel reinforcement ratio, (b) lengths of SMA bars, (c) elastic modulus of SMA, (d) compressive strength of concrete, and (e) axial load applied on the column. The numerical results of this study are expected to enrich the database on smart materials, and encourage the scientific community to explore their potential applications in various structures.

2. Experimental Reference

The laboratory experiments performed by Youssef et al. [19] were used as an accredited reference for the present numerical investigation. Youssef's study considered the effect of using SMA on the seismic behavior of external RC beam column joints using two ¾ scale specimens. The first specimen (steel-BCJ) was well seismically designed and reinforced with steel reinforcement, whereas the second specimen (SMA-BCJ) was partially reinforced with SMA bars in the plastic hinge of the beam as shown in Figure 1. Their test results exhibited very small residual displacements for reinforced (SMA-BCJ) joints compared to the corresponding displacements of the conventional steel-RC beam–column joint (steel-BCJ), as shown in Figure 2. Moreover, the use of SE-SMA bars in the joint region successfully relocated the plastic hinge region away from the face of the column to a distance of approximately half the beam depth. It is observed from Figure 2 that the SMA-BCJ dissipated less energy compared to steel-BCJ. However, the energy dissipated by the SMA-BCJ could be equivalent to that of steel-BCJ, and enhanced further by optimizing the use of steel bars in conjunction with SMA bars as shown in the following sections.

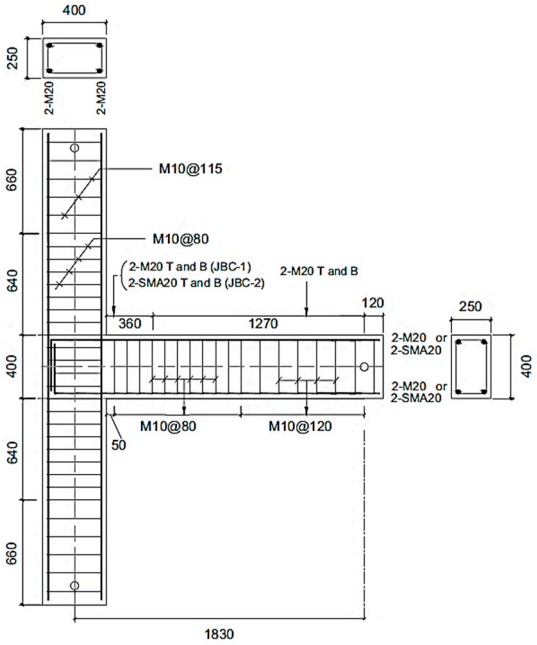

Figure 1. Reinforcement details of specimens, steel-BCJ and SMA-BCJ (all dimensions in mm). Reprinted from [19], with permission from Taylor and Francis.

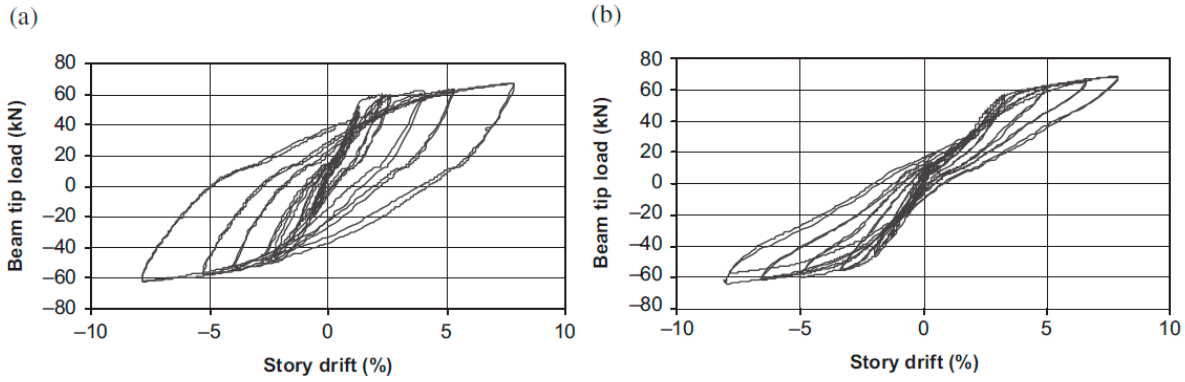

Figure 2. Beam tip load–story drift relationship of specimens: (**a**) steel-BCJ and (**b**) SMA-BCJ. Reprinted from [19], with permission from Taylor and Francis.

3. Finite Element Modelling

Three-dimensional (3D) nonlinear finite element models were developed in ABAQUS and validated by experimental data for the RC-BCJ investigated. The elements, interactions, boundary conditions, and materials are explained in the subsequent sections.

3.1. Elements, Interactions, and Boundary Conditions

The modeling of the RC-BCJ includes modeling the concrete, steel and SMA reinforcements. An 8-node solid (C3D8R), and two-node truss elements (T3D2) were, respectively, employed for modeling concrete and rebars of RC joints. The steel and SMA reinforcement were modeled assuming a perfect bond between steel and concrete, and thus embedded region interaction was employed, as shown in Figure 3a,b. Tie contact was used to simulate the coupler contact between steel and SMA bars. The discretized mesh of the RC-BCJ is shown in Figure 3c. The pin and roller supports at both ends of columns were modelled in ABAQUS to simulate the boundary conditions of the experimental study. In addition, the reference points were assigned to calculate the reaction forces easily from the supports during the test as shown in Figure 4. As reported by many researchers [20,26–29], the pinching effect is a limitation for embedded constraint in ABAQUS software and could not be addressed in simulating the cyclic performance of RC structures. Therefore, in this investigation, a monotonic load was applied at the tip of the beam, in addition to a constant axial load applied at the end of the column, equals to 15% of the column capacity.

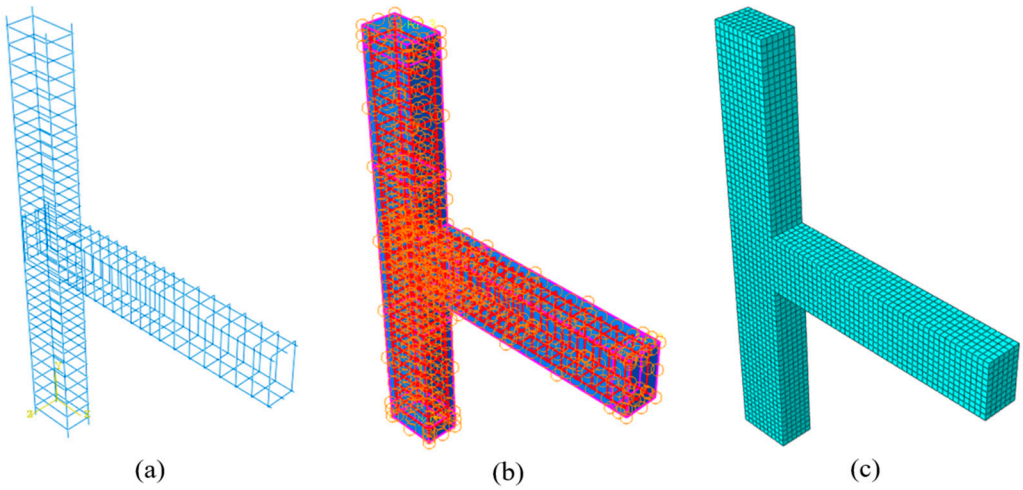

Figure 3. (**a**) Reinforcement of RC beam column joint. (**b**) Embedded region contact between concrete and reinforcement. (**c**) Typical finite element mesh of RC-BCJ.

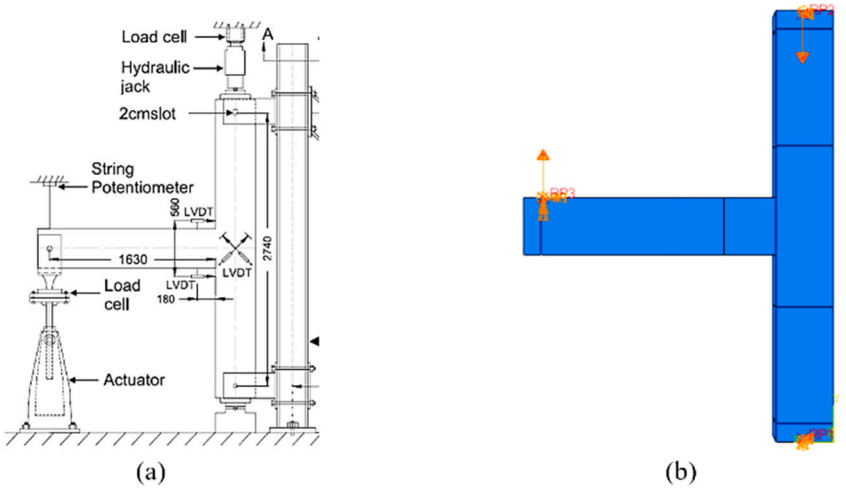

Figure 4. Boundary conditions of RC-BCJ: (**a**) experimental, reprinted from [19], with permission from Taylor and Francis. (**b**) Numerical.

3.2. Materials Models

In the numerical study, the concrete damage–plasticity available in ABAQUS was employed to model the inelastic behavior of concrete. The plasticity parameters of concrete are presented in Table 1. The materials properties of steel, concrete and SMA were obtained from the experimental study conducted by Youssef et al. [19] for validation purposes. As reported in their study, concrete compression and tensile tests were performed for both samples, steel-BCJ and SMA-BCJ. In addition, the yield and ultimate strength of steel rebars were based on the laboratory tensile test results reported in reference [19]. Moreover, the SMA properties were also obtained from the same reference based on the experimental cyclic tensile tests with couplers at room temperature. The compressive strength and modulus of elasticity of concrete were 53 MPa and 31,179 MPa, respectively. The isotropic plasticity behavior was assumed to model the steel reinforcement. The yield and ultimate strengths of longitudinal steel rebars were 450 and 650 MPa, respectively, and 422 MPa and 682 MPa for transverse steel reinforcement, respectively. The modulus of elasticity and Poisson's ratio of steel rebars were 193 GPa and 0.3, respectively. The density of concrete and steel were taken as 2.4×10^{-9} and 7.85×10^{-9} ton/mm^3, respectively. The SMA bars were defined using the newly built-in superelasticity model in ABAQUS version 2019 and newer [21], as shown in Figure 5. The definition of superelasticity in ABAQUS is based on the constitutive relationship proposed by Auricchio and Taylor work [34,35]. Their model was capable of describing the force–deformation relationship of SMA as demonstrated in the numerical studies performed by Shrestha and Hao [32], and Fugazza [36]. The parameters used to define the SMA bars in this investigation were obtained from the experimental cyclic load test carried out by Youssef et al. [19], as shown in Table 2.

Table 1. Parameters of damage–plasticity model.

Dilation Angle	Eccentricity	fb_0/fc_0	k	Viscosity Parameter
40	0.1	1.16	0.667	0

Table 2. Mechanical properties of SMA bars used in ABAQUS.

Start of Transformation (Loading) σ^s_{tL}	End of Transformation (Loading) σ^E_{tL}	Start of Transformation (Unloading) σ^s_{tU}	End of Transformation (Unloading) σ^E_{tU}	Young's Modulus E_A	Transformation Strain ε^L
450 MPa	500 MPa	350 MPa	180 MPa	32,000 MPa	0.055

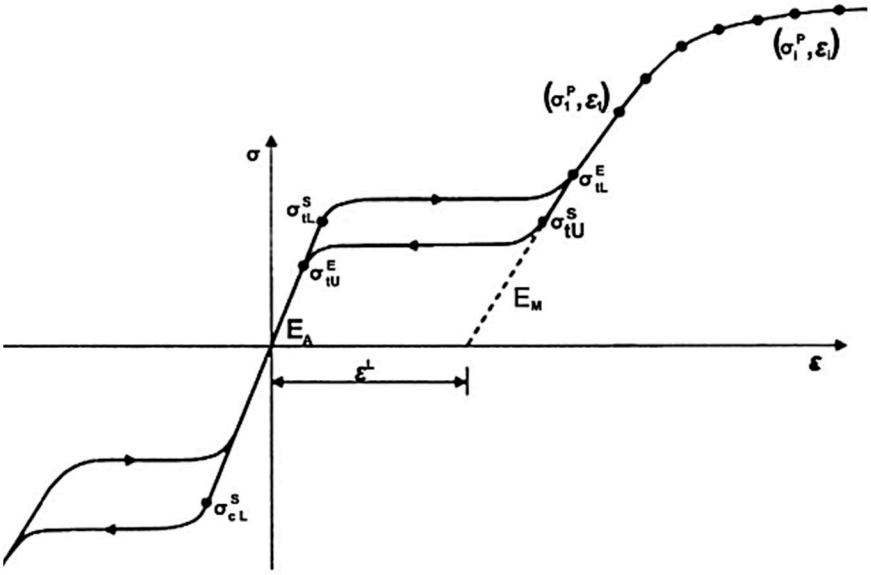

Figure 5. Performance of superelastic material under uniaxial tension (ABAQUS Manual). Reprinted from [21], with permission from Creative Commons Attribution (CC BY) license.

4. Model Validation

The first stage in this study was the validation of the numerical models developed in ABAQUS using the experimental test results obtained by Youssef et al. [19]. Sensitivity analysis was carried out to determine the optimum mesh size required for simulating the performance of RC-BCJ and validating the experimental results. Different mesh sizes ranging from 50 mm to 20 mm were investigated. Table 3 presents the numerical peak loads for these mesh sizes along with the corresponding ratios of numerical to experimental peak loads. The analysis demonstrated that, decreasing the mesh size beyond 30 mm had a negligible effect on the response values and thus, this value represents the optimum mesh size that satisfies the accuracy and computational time. The mesh size used for concrete and reinforcement elements was 30 mm, with a total number of elements equal to 11,967.

Table 3. Effect of mesh size on peak load.

Mesh Size (mm)	Number of Elements	Numerical Peak Load (kN)	Ratio of Numerical to Experimental Peak Loads
50	5387	72.4	1.112
40	9139	69.8	1.072
30	11,967	66.3	1.018
20	66,521	65.9	1.012

Figure 6 provides comparisons between the numerical and experimental results for the joints reinforced by steel rebars (steel-BCJ) or SMA bars (SMA-BCJ). The numerical results seem to be closely matching the experimental test results. The comparison of the experimental and numerical values of peak load, stiffness, and energy dissipation for steel-BCJ and SMA-BCJ samples are shown in Table 4. It is observed that the numerical values match well with the experimental results and the numerical model was capable of predicting the response of joints with errors varied between 0.25% and 3.08%. Following the validation of the model developed, a parametric investigation was carried out to determine the most influential parameters on the seismic response of the joint.

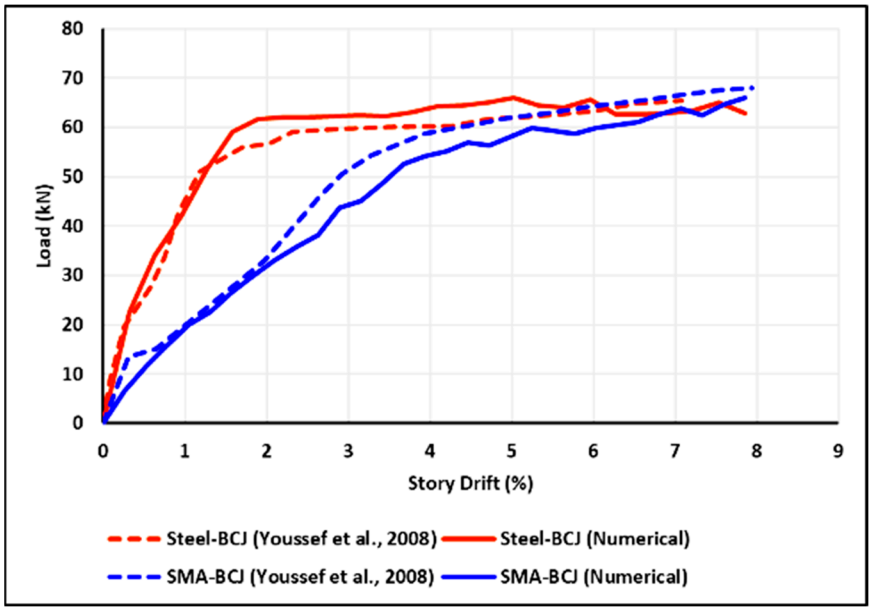

Figure 6. Experimental and numerical beam tip-load versus story drift envelope for the specimens steel-BCJ and SMA-BCJ [19].

Table 4. Comparison between the numerical and experimental values for the RC-BCJ tested.

Sample ID	Steel-BCJ			SMA-BCJ		
	Numerical	Expermintal	Error	Numerical	Expermintal	Error
Peak Load (kN)	65.1	66.3	−1.81%	66.0	68.1	−3.08%
Stiffness (kN/mm)	5.05	4.92	+2.64%	1.78	1.83	−2.73%
Energy dissipation (kN/m)	4154	4187	−0.79%	3580	3571	+0.25%

5. Numerical Study

To investigate the effect of different ratios of SMA to steel rebars on the behavior of RC beam column-joint, the joint reinforcement designed by Youssef et al. [19] was changed from 2Ø20 mm (As = 628 mm^2) to 3Ø16 mm (As = 603 mm^2). A typical layout of the various reinforcement details proposed in this study are presented in Figure 7. The numerical results obtained from the finite element analysis using ABAQUS are shown in Figures 8–12. They included three-dimensional views of the reinforcement and their stress distribution, comparison of the load displacement curves, stress at the middle of the bottom rebars versus the span of the beam, comparison between the stresses in steel and SMA bars along the span of the beam, and a comparison between the load applied at the tip of the beam versus the story drift. It is observed from the figures that the numerical load–deflection relationships were similar to the experimental test results obtained by Youssef et al. [19]. The stress distributions in the reinforcement along the span of the beam proved that the use of SMA bars in the plastic hinge region prevented the yielding of steel rebars and thus eliminated the risk of permanent deformations. Moreover, the numerical results indicated that the minimum length of SMA bars required to avoid high stresses in the couplers between the SMA bars and steel bars is approximately 360 mm. Beyond that length, yielding of steel bars can be avoided, and failure of the joint and post-maintenance requirements can be alleviated. It should be noted that the length of SMA bars used by Youssef et al. [19] was conservative and long enough to contain the plastic hinge region. Therefore, the structural designers should choose carefully couplers with a strength capacity higher than that of steel and SMA bars to avoid any unexpected failure mode in the coupler.

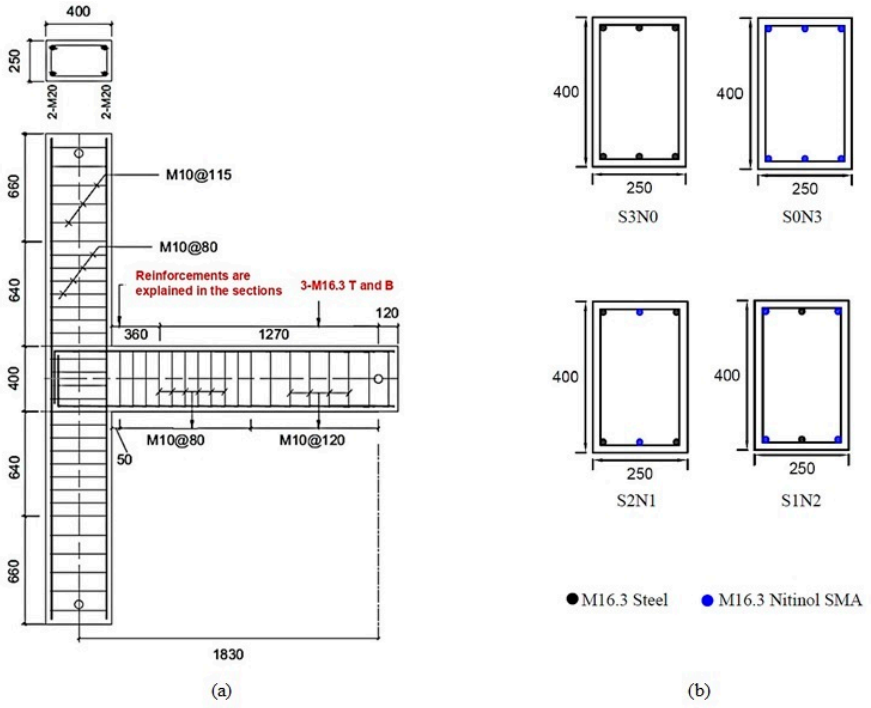

Figure 7. (**a**) Typical reinforcement details of the specimens. (**b**) Reinforcement details at the plastic hinge of RC-BCJ specimens (all dimensions in mm).

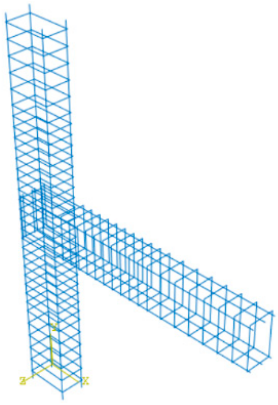

Figure 8. Reinforcement RC-BCJ as obtained from FE.

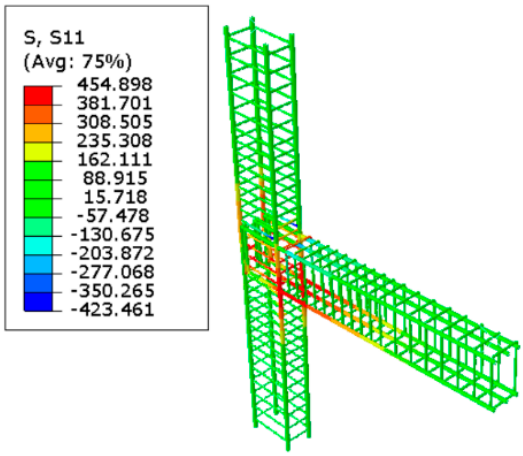

Figure 9. Stress in the reinforcement RC-BCJ as obtained from FE.

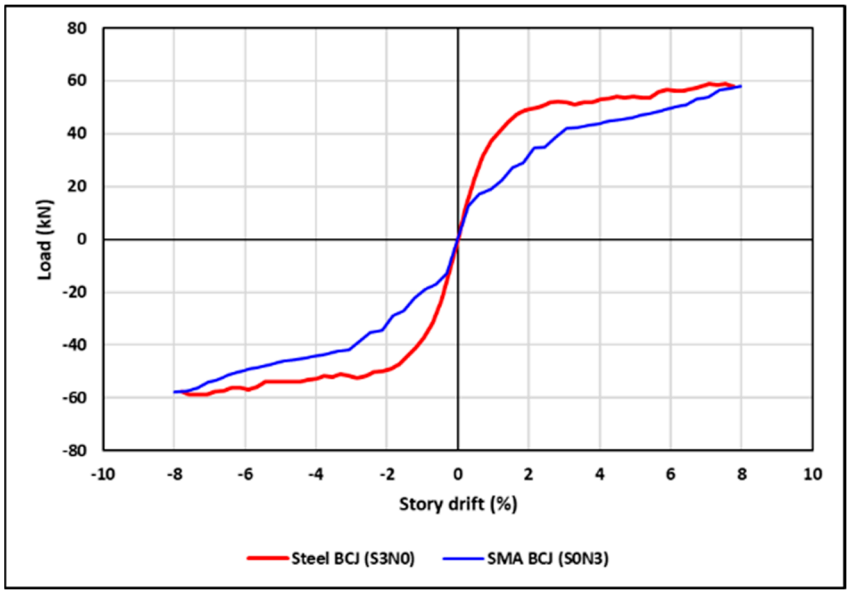

Figure 10. Numerical beam tip-load versus story drift envelope of the specimens C25-A0-S3N0 and C25-A0-S0N3.

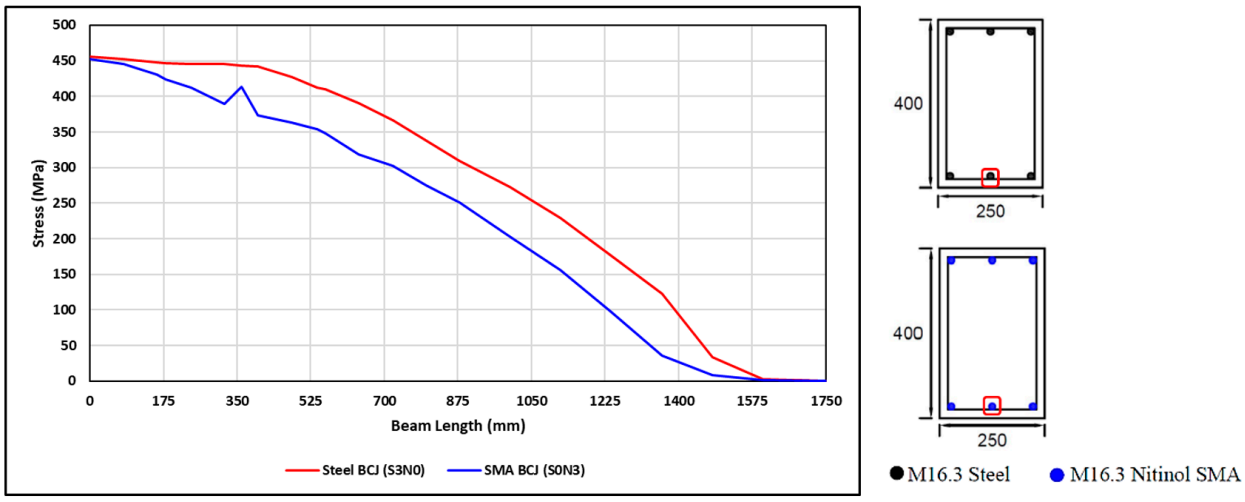

Figure 11. Stress of the beam reinforcement rebar under monotonic pull loading versus the span length of the beam at 8% drift.

The details and designations of the parameters influencing the response of the RC-BCJ investigated numerically are listed in Tables 5 and 6. The definition of concrete damage–plasticity model parameters for 25 MPa, 40 MPa and 70 Mpa concretes are presented in Figure 13. All the specimens were tested under monotonic load applied at the tip of the beam up to a drift ratio of 8%. The applied load versus deflection were recorded for push and pull directions to compare the response of the joints in terms of load capacity, stiffness, and energy dissipation. As a measure of the energy dissipation of the specimens, the area under the load–displacement envelopes were computed and defined as the energy that could be dissipated by the specimens before the system loses its stability [37,38]. The secant stiffness was calculated from the slope of the line drawn between the origin and a point on the envelope corresponding to 40% of the ultimate load.

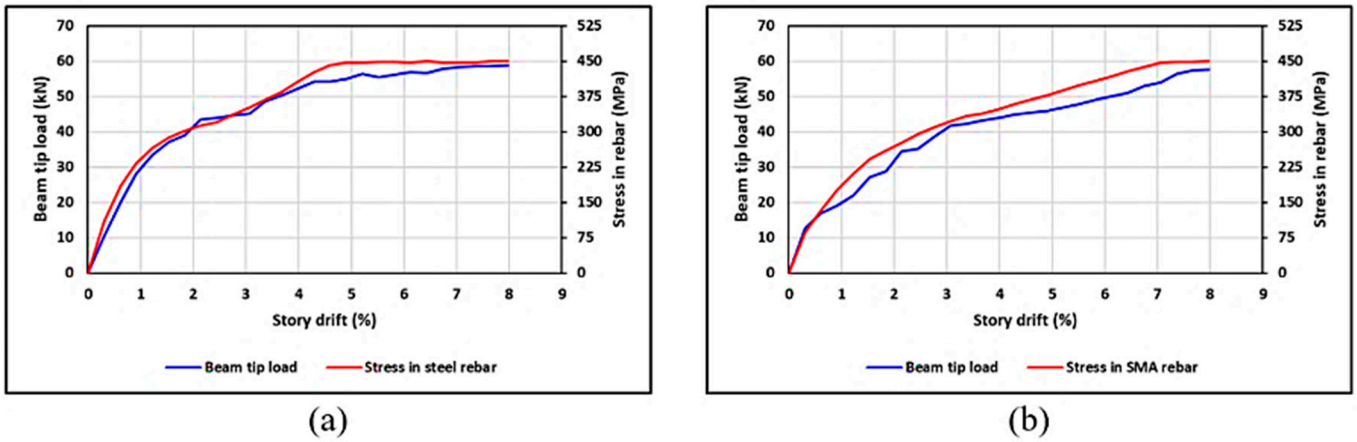

Figure 12. Comparisons of the numerical beam tip load and stresses in rebars versus story drift of the specimens: (**a**) C25-A0-S3N0 and (**b**) C25-A0-S0N3.

Table 5. The parameters used in the numerical investigation.

Parameter	Values		
SMA–steel Reinforcement Ratio	S2N1	S1N2	S0N3
Length of SMA (mm)	180	360	540
Elasticity of SMA (Gpa)	32	57	82
Concrete Strength (MPa)	25	40	70
Axial Load Level (%)	15%	30%	60%

Table 6. Details of the specimens used in the numerical investigation.

#	Parameters	Specimen ID *	Concrete Strength (Mpa)	Axial Load Level	Steel Rebars	Nitinol SMA Rebars	Elastic Modulus of SMA (Gpa)	Length of SMA (mm)
1	Control	C25-A0-S3N0	25	0%	3Ø16	-	-	-
2		C25-A0-S0N3	25	0%	-	3Ø16	32	360
3	SMA–Steel Reinforcement	C25-A0-S1N2	25	0%	1Ø16	2Ø16	32	360
4		C25-A0-S2N1	25	0%	2Ø16	1Ø16	32	360
5	Length of SMA	C25-A0-S0N3-L180	25	0%	-	3Ø16	32	180
6		C25-A0-S0N3-L540	25	0%	-	3Ø16	32	540
7	Elastic Modulus of SMA	C25-A0-S0N3-E57	25	0%	-	3Ø16	57	360
8		C25-A0-S0N3-E82	25	0%	-	3Ø16	82	360
9	Concrete Compressive Strength	C40-A0-S3N0	40	0%	3Ø16	-	-	-
10		C70-A0-S3N0	70	0%	3Ø16	-	-	-
11		C40-A0-S0N3	40	0%	-	3Ø16	32	360
12		C70-A0-S0N3	70	0%	-	3Ø16	32	360
13	Axial Load Level	C25-A15-S3N0	25	15%	3Ø16	-	-	-
14		C25-A30-S3N0	25	30%	3Ø16	-	-	-
15		C25-A60-S3N0	25	60%	3Ø16	-	-	-
16		C25-A15-S0N3	25	15%	-	3Ø16	32	360
17		C25-A30-S0N3	25	30%	-	3Ø16	32	360
18		C25-A60-S0N3	25	60%	-	3Ø16	32	360

* C: concrete strength, A: axial load level, S: number of steel rebars, N: number of nitinol SMA rebars, E: elastic modulus of SMA, and L: length of SMA.

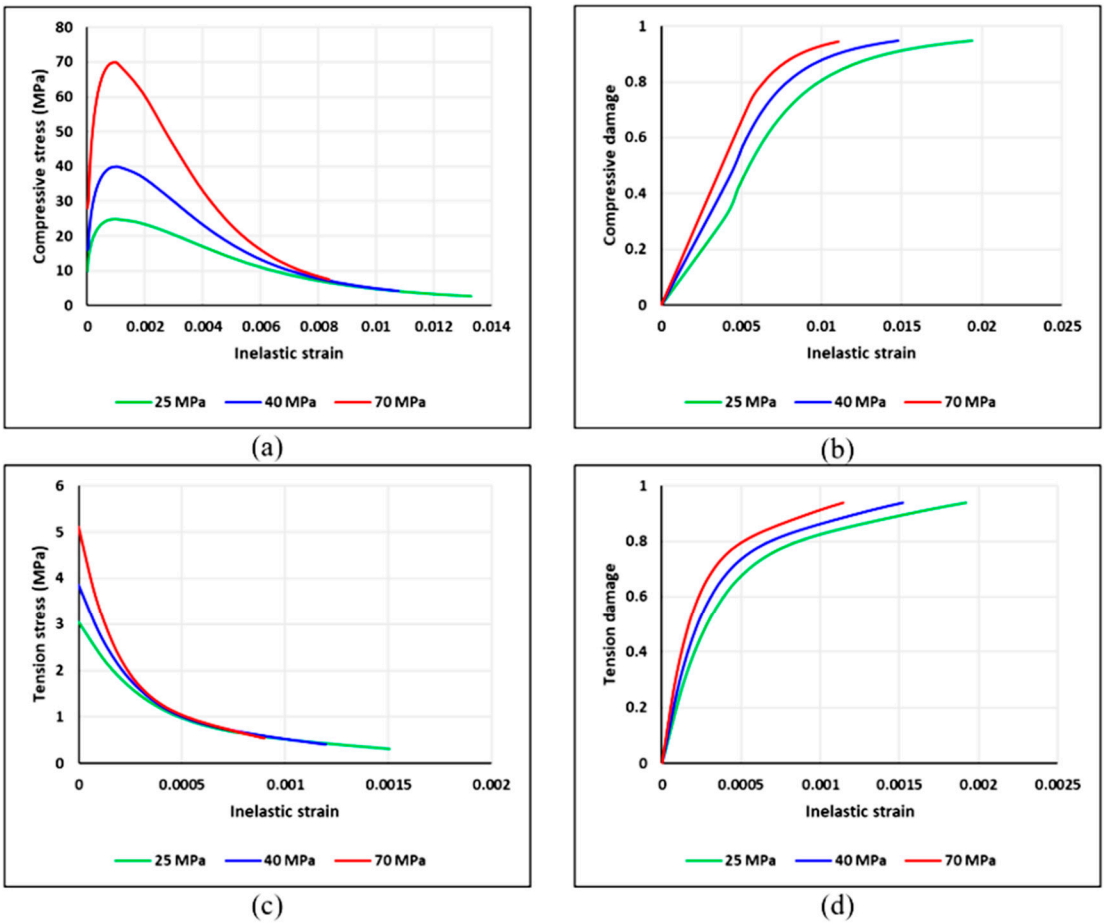

Figure 13. Definition of concrete damage–plasticity model parameters in ABAQUS: (**a**) compressive stress vs. inelastic strain, (**b**) compressive damage vs. inelastic strain, (**c**) tensile stress vs. cracking strain, and (**d**) tensile damage vs. cracking strain.

6. Parametric Study

Parameters investigated included the effect of the SMA–steel reinforcement ratio, lengths of SMA bars, elastic modulus of SMA bars, compressive strength of concrete, and the column axial load, on the structural response of the RC-BCJ. The structural response was investigated in terms of load carrying capacity, stiffness, and energy dissipation. The details of the numerical parameters investigated are presented in Table 5; they were selected based on the findings of previous research studies. First, the level of the partial replacement of steel reinforcement with SMA bars was chosen by referring to the results reported in the literature in this field [4–6,19,20]. This level is important for mitigating the residual displacement of the joint without sacrificing the energy dissipation of the structure. Second, the range of the elastic modulus for SMA bars was selected based on the test results reported by some researchers [8,19,33]. This range had an important effect on the stiffness of the RC joint itself. Third, the length of the SMA bars necessary for enhancing the superelastic response of the joint without reducing its energy dissipation characteristics was also decided upon in a similar way. Fourth, the range of concrete compressive strength shown in Table 5 was chosen in order to cover the behavior of most commonly used concrete in practice. This range had a significant impact on the performance of the structure as reported by many researchers [19,20,23,33]. Finally, the axial load levels were chosen in order to simulate the actual load levels expected to act in real structures. These load levels were comparable to those reported by some other researchers [39–42].

In the current study, the performance of RC beam column joints was investigated by using SMA as main reinforcement in the plastic hinge not for strengthening. Additionally,

the position of SMA bars as a reinforcement was investigated in terms of two parameters: the length of SMA, and the partial replacement of steel reinforcement with SMA bars. Three lengths of SMA bars, 180 mm, 360 mm, and 540 mm, corresponding to 10%, 20% and 30% of the span of the beam, respectively, were investigated. For partial replacement of steel reinforcement with SMA bars: one sample was tested using the SMA bar in the middle and the other two steel bars on the sides (S2N1). The second sample was tested using two SMA bars on the sides and one steel bar in the middle (S0N2). This approach was implemented in order to resolve the issue of lower energy dissipation of the RC joints reported by some other researchers.

6.1. Effect of SMA–Steel Reinforcement Ratio

SMA bars were used in conjunction with steel rebars at two different reinforcement ratios in order to take full advantage of the self-centering (displacement recovery) and ductility provided by the SMA and the high energy dissipation provided by the steel. Two joint specimens were investigated, the first one (S2N1) was reinforced by two steel rebars and one SMA bar, whereas the second one (S1N2) was reinforced by one steel rebar and two SMA bars. The numerical results of these specimens were compared with control specimens reinforced with three steel rebars only (S3N0), and three SMA bars only (S0N3). The concrete strength of all the specimens was taken as 25 MPa; monotonic load was applied at the tip of the beam, and no axial column load was used.

The load–drift curves of specimens C25-A0-S3N0, C25-A0-S1N2, C25-A0-S2N1, C25-A0-S0N3 are shown in Figure 14. It is observed that the SMA–steel reinforcement system improved the stiffness and energy dissipation of RC-BCJ compared to control specimens. All specimens achieved the same peak load capacity, regardless of the type of reinforcement used in the joint. Moreover, the use of the SMA–steel reinforcement system enhanced the stiffness of S1N2, and S2N1 compared to S0N3 by 92% and 108%, respectively. A similar trend was also observed for the energy dissipation variation between the specimens, as shown in Figure 15c.

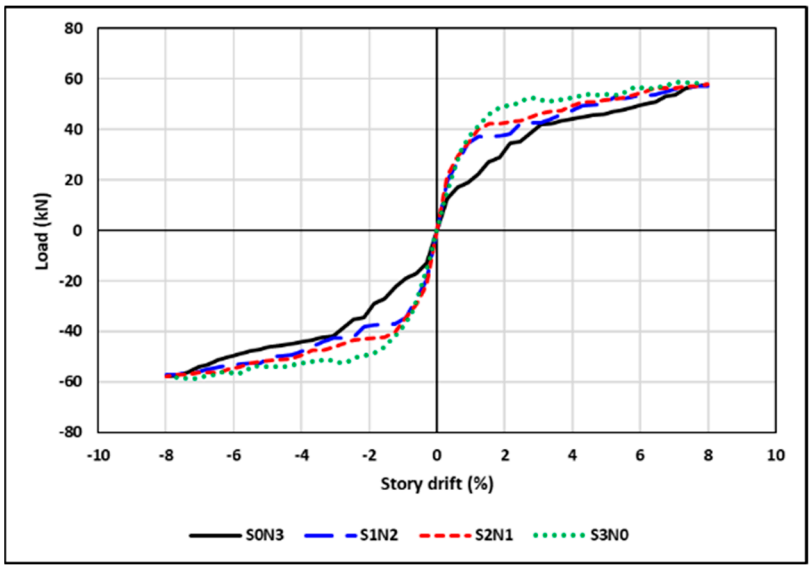

Figure 14. Numerical beam tip-load versus story drift envelopes of the C25-A0-S3N0, C25-A0-S1N2, C25-A0-S2N1, and C25-A0-S0N3 specimens.

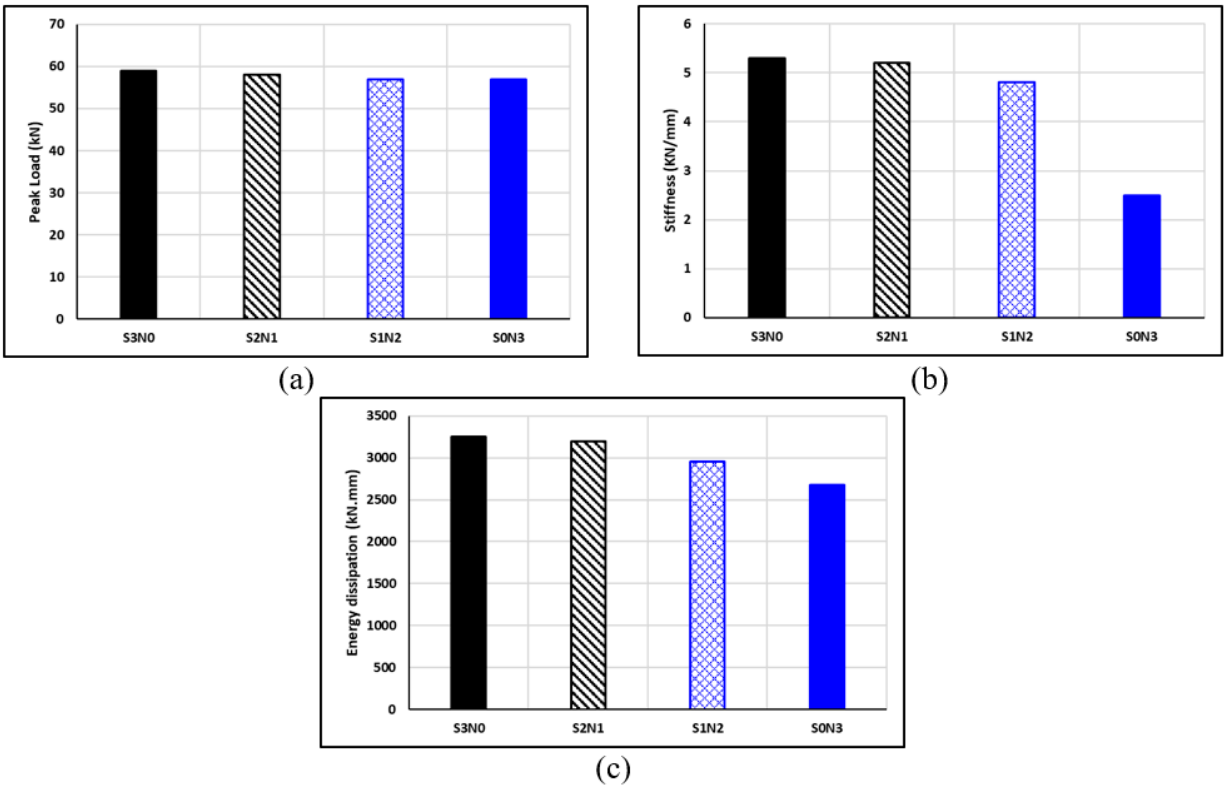

Figure 15. Effect of SMA-steel reinforcement ratios of the BCJ on (**a**) load capacity, (**b**) stiffness, and (**c**) energy dissipation.

The energy dissipation of specimen S1N2 and S2N1 were increased by 10% and 19%, respectively, compared to control specimen S0N3. For the drift ratios assumed (2.8% and 8%), higher stresses over a long distance from the face of the column were observed in the steel rebars compared to the SMA bars as shown in Figures 16 and 17. This is due to the higher axial stiffness of the steel 200 GPa vs. 32 GPa for the SMA. The joint is likely to experience yielding and inelastic deformations at the plastic hinge regions if the joints are fully reinforced with steel rebars. This situation is improved when SMA bars are used in conjunction with steel reinforcement. As mentioned earlier, the SMA–steel reinforcement system enhanced the stiffness, energy dissipation, and drift recovery by taking full advantage of self-centering and higher stiffness of SMA and steel, respectively.

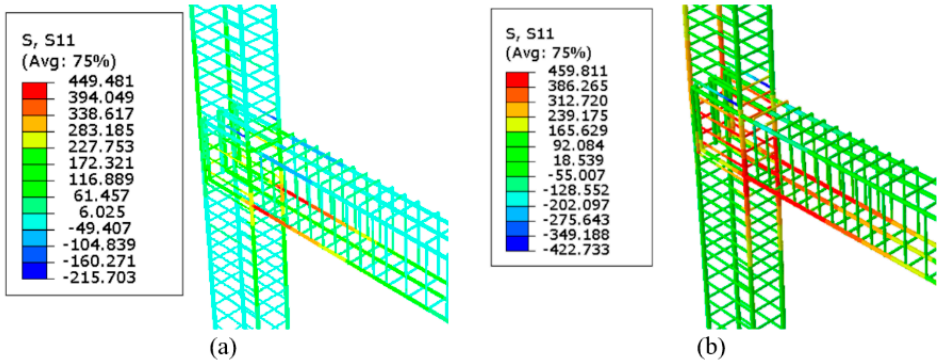

Figure 16. Stresses of steel and SMA rebars of S2N1 specimen during push loading at (**a**) 2.8% story drift and (**b**) 8% story drift.

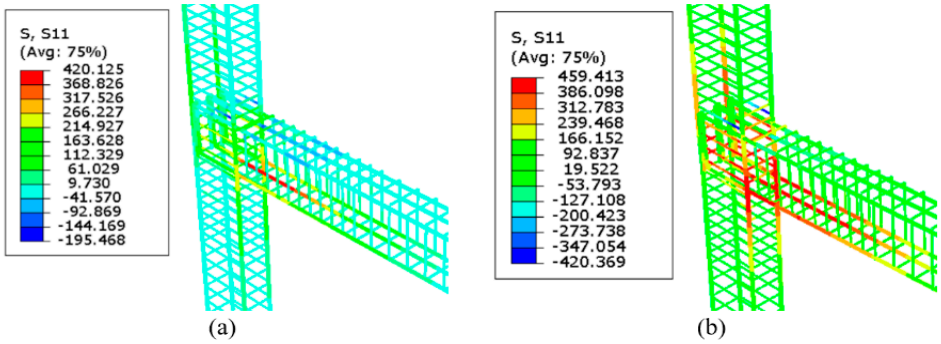

Figure 17. Stresses of steel and SMA rebars in S1N2 specimen during push loading at (**a**) 2.8% story drift and (**b**) 8% story drift.

6.2. Effect of SMA Bar Length

The required length of SMA bars in the plastic hinge region is one of the challenges in designing RC-BCJ. This study investigated the effect of changing SMA bar lengths on the performance of joint specimens designated as C25-A0-S0N3. Lengths used are 180, 360, and 540 mm, which correspond to 10%, 20% and 30%, of the span of the beam, respectively. The effect of SMA bar length on the stress in the reinforcements versus the span of the beam for specimens C25-A0-S0N3-L180, C25-A0-S0N3 and C25-A0-S0N3-L540 are presented in Figure 18. It can be observed that the stresses in the steel reinforcement reached yielding within a distance of up to 300 mm away from the face of the column. The results indicated also that the use of SMA bars with length less than 300 mm may not guarantee the prevention of steel yielding. It is worth mentioning herein that the couplers region in the three cases had high stresses compared to the connected SMA and steel bars. This should be an important aspect during the design stage of the joints reinforced by SMA bars to eliminate the risk of sudden failure in the couplers. The load–displacement curves shown in Figure 19 indicated that the increase in SMA bar length had insignificant effect on the load capacity and a slight effect on the energy dissipation. However, the use of a shorter length of SMA bars increased the joint stiffness, as shown in Figure 20b. The longer length of steel bars would have higher stiffness than SMA bars.

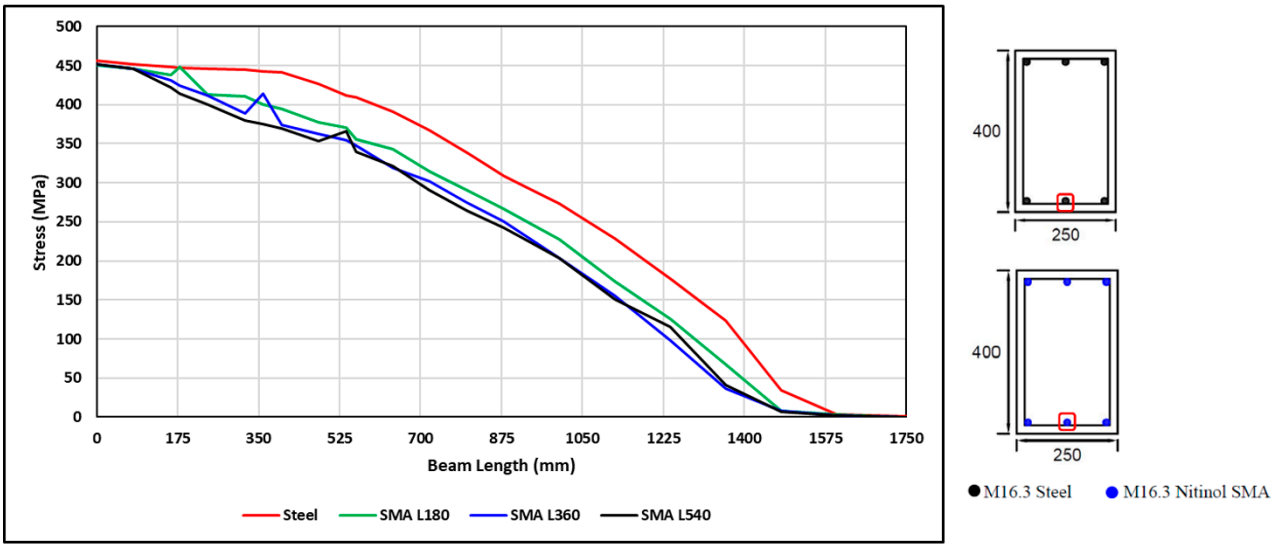

Figure 18. Stress of the beam reinforcement rebar using different lengths of SMA under monotonic pull loading versus the beam length at 8% drift.

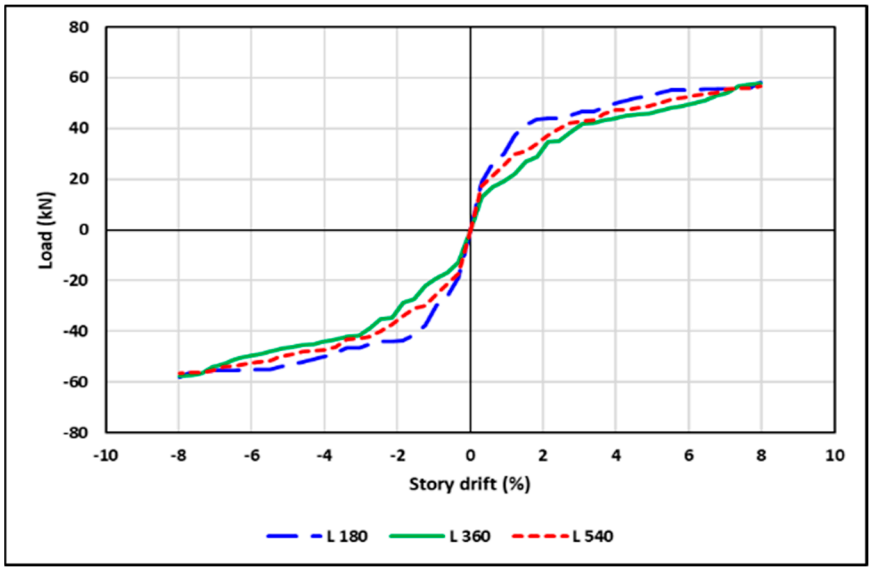

Figure 19. Numerical beam tip-load versus story drift envelopes of the specimens C25-A0-S0N3, C25-A0-S0N3-L180 and C25-A0-S0N3-L540.

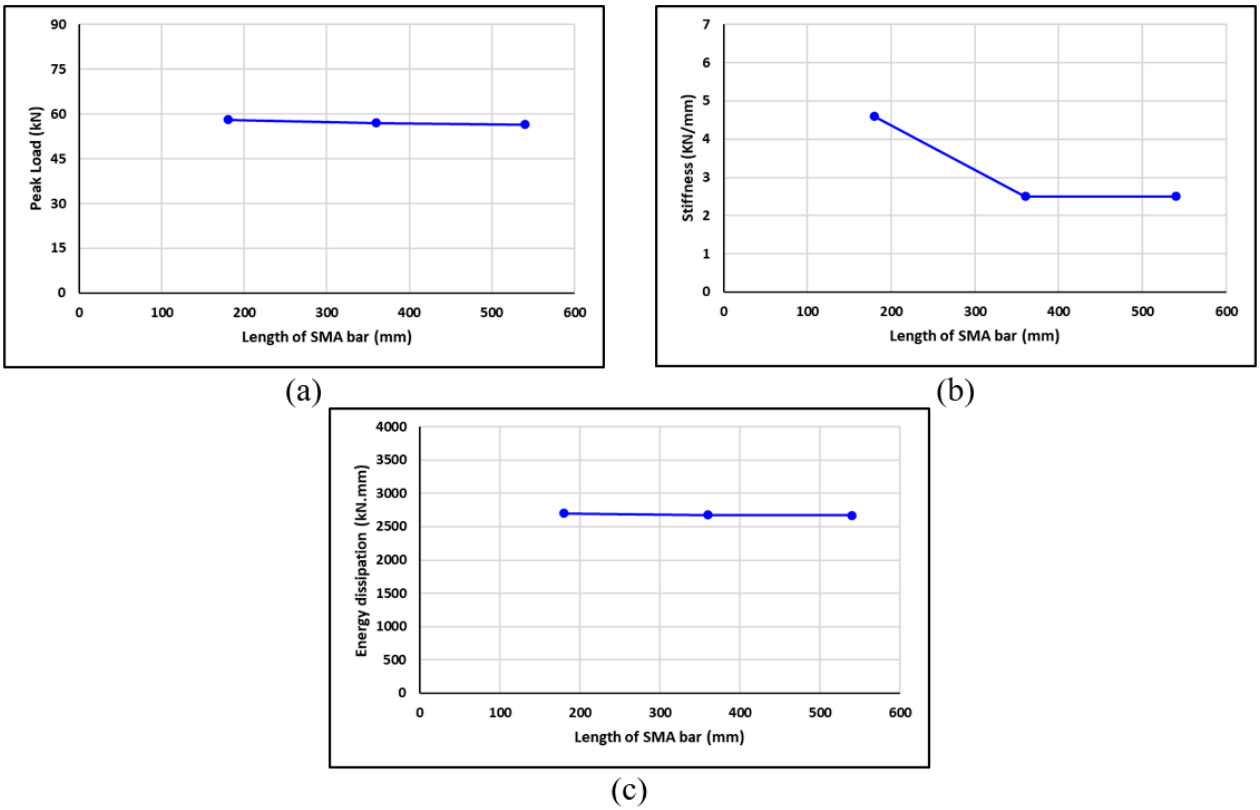

Figure 20. Effect of SMA bar length of the BCJ on (**a**) load capacity, (**b**) stiffness, and (**c**) energy dissipation.

6.3. Effect of SMA Elastic Modulus

Elastic modulus of SMA is Young's Modulus in the austenite phase. It is one of the most important parameters that affects the self-centering capability of SMA in the elastic stage. There are different types of SMA with different values of elastic modulus. The nitinol SMA could have elastic modulus varying between 30 and 90 GPa [43–45] based on the chemical combinations. The elastic modulus of SMA type used by Youssef et al. [19] and this study was 32 GPa. Two additional values of the elastic modulus of SMA, 57 and

82 GPa were investigated by keeping all other parameters constant. The numerical results of C25-A0-S0N3, C25-A0-S0N3-E57 and C25-A0-S0N3-E82 specimens are illustrated in Figure 21. The numerical results shown in Figure 22a indicated that the increase in the elastic modulus of SMA had no effect on the peak load of RC-BCJ. However, increasing the elastic modulus from 32 to 57 GPa, resulted in enhancing the stiffness and energy dissipation of the joint by 48% and 12%, respectively. A further increase in the modulus of elasticity from 57 to 82 GPa had a slight effect on the stiffness and almost no effect on energy dissipation, as seen from Figure 22b,c.

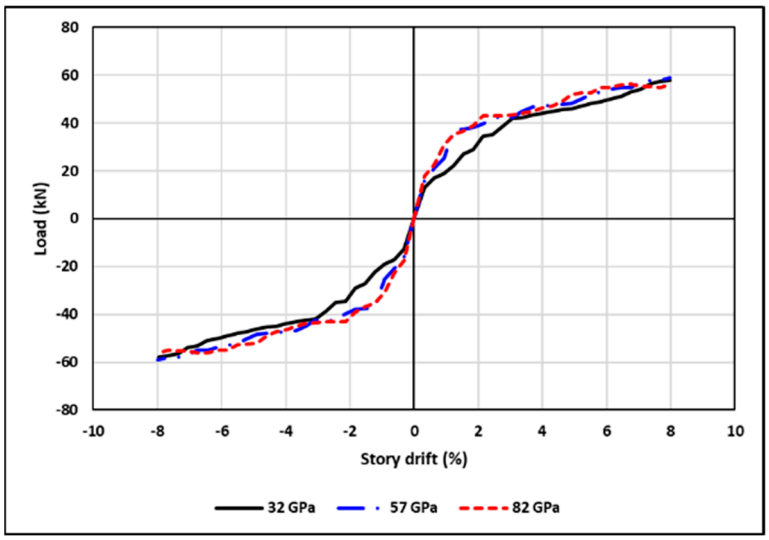

Figure 21. Numerical beam tip-load versus story drift envelope of the specimens C25-A0-S0N3, C25-A0-S0N3-E57 and C25-A0-S0N3-E82.

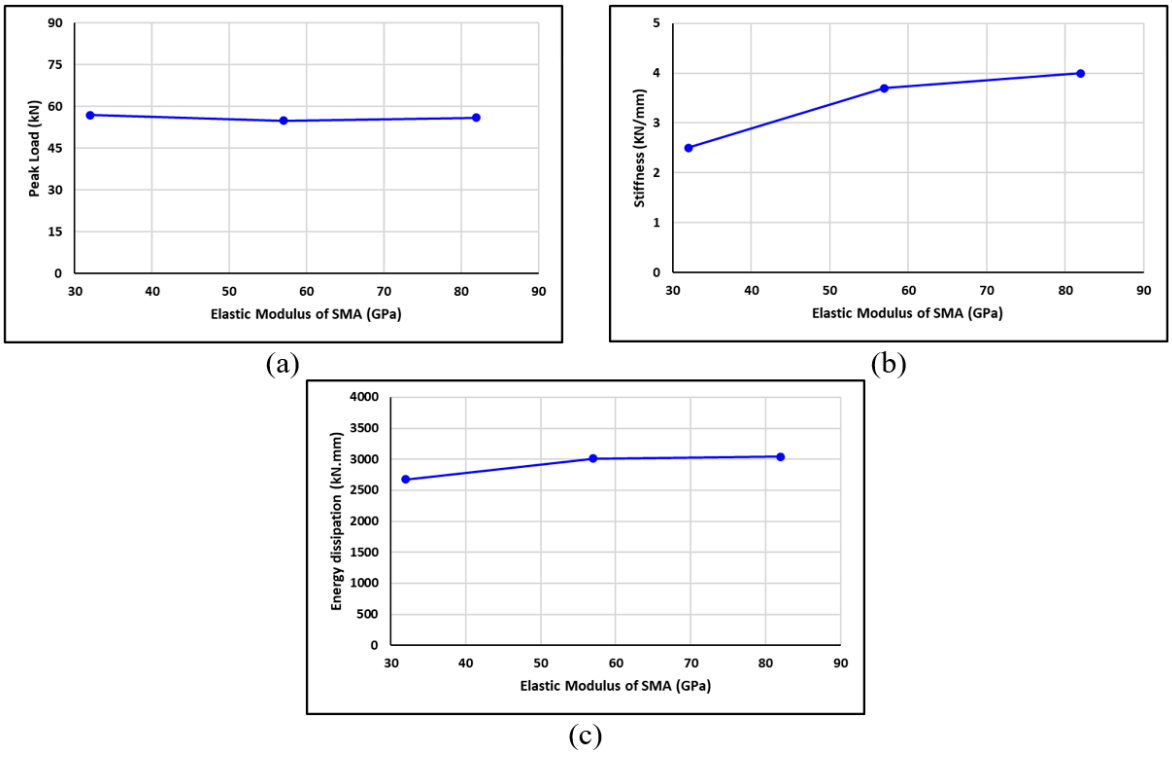

Figure 22. Effect of SMA elastic modulus of the BCJ on (**a**) load capacity, (**b**) stiffness, and (**c**) energy dissipation.

6.4. Effect of Concrete Strength

The effect of the compressive strength of concrete on the behavior of RC-BCJ was investigated considering three compressive strength grades of 25, 40, and 70 MPa, by keeping all other parameters constant. The C25-A0-S3N0, C40-A0-S3N0 and C70-A0-S3N0 specimens studied the effect of concrete strength on the behavior of BCJ reinforced with steel rebars, while the C25-A0-S0N3, C40-A0-S0N3 and C70-A0-S0N3 specimens considered the BCJ reinforced with SMA bars. The effect of compressive strength of concrete on the response of BCJ specimens reinforced with steel and SMA bars are illustrated in Figures 23a and 23b, respectively. In general, the increase in concrete compressive strength resulted in an increase in the load capacity, stiffness, and energy dissipation of the joint as shown in Figures 23 and 24. Increasing the concrete compressive strength from 25 to 40 MPa and from 25 to 70 MPa enhanced the load capacity by 20% and 36% for BCJ reinforced with steel rebars, respectively. A similar trend for the peak load was also observed for the BCJ reinforced with SMA, as observed from Figure 25a. As expected, the BCJ reinforced with SMA bars exhibited lower stiffness and energy dissipation compared to the BCJ reinforced with steel bars. Meanwhile, increasing the concrete strength from 25 to 40 MPa and from 25 to 70 MPa resulted in a significant improvement in the stiffness by 123% and 162% for steel joints, respectively, and by 52% and 136% for SMA joints, respectively, as shown in Figure 25b. Moreover, the energy dissipated by the joint reinforced with steel increased by 35% and 48% when the concrete strength was increased from 25 MPa to 40 and 70 MPa, and by 22% and 34% for the joints reinforced with SMA when the concrete strength was increased from 25 to 40 and 70 MPa as shown in Figure 25c.

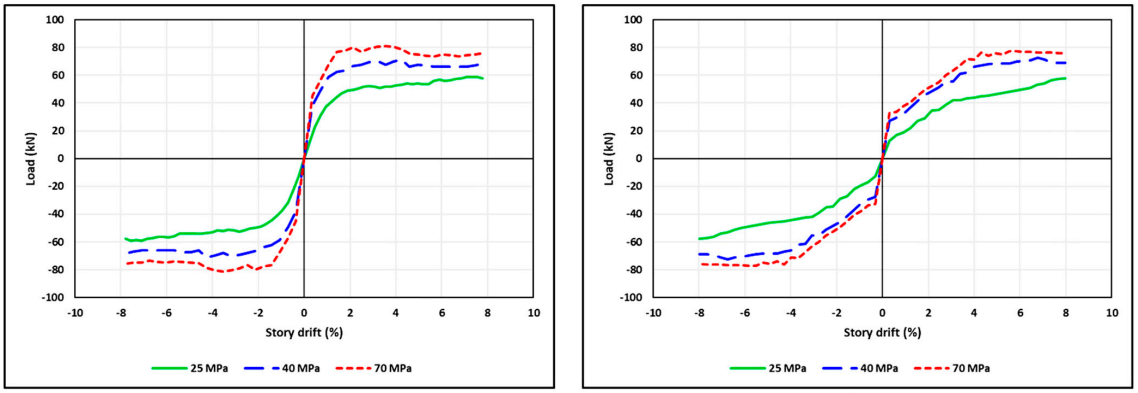

Figure 23. Numerical beam tip-load versus story drift envelopes of the specimens (**a**) C25-A0-S3N0, C40-A0-S3N0 and C70-A0-S3N0 (**b**) C25-A0-S0N3, C40-A0-S0N3 and C70-A0-S0N3.

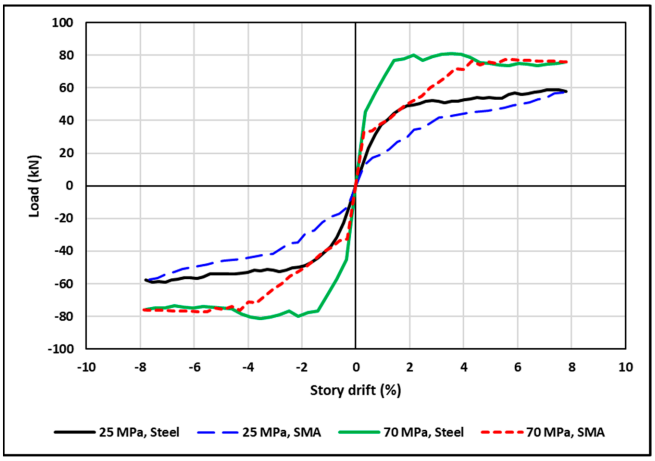

Figure 24. Comparison of effect of concrete strength on the behavior of BCJ between reinforced with steel and SMA.

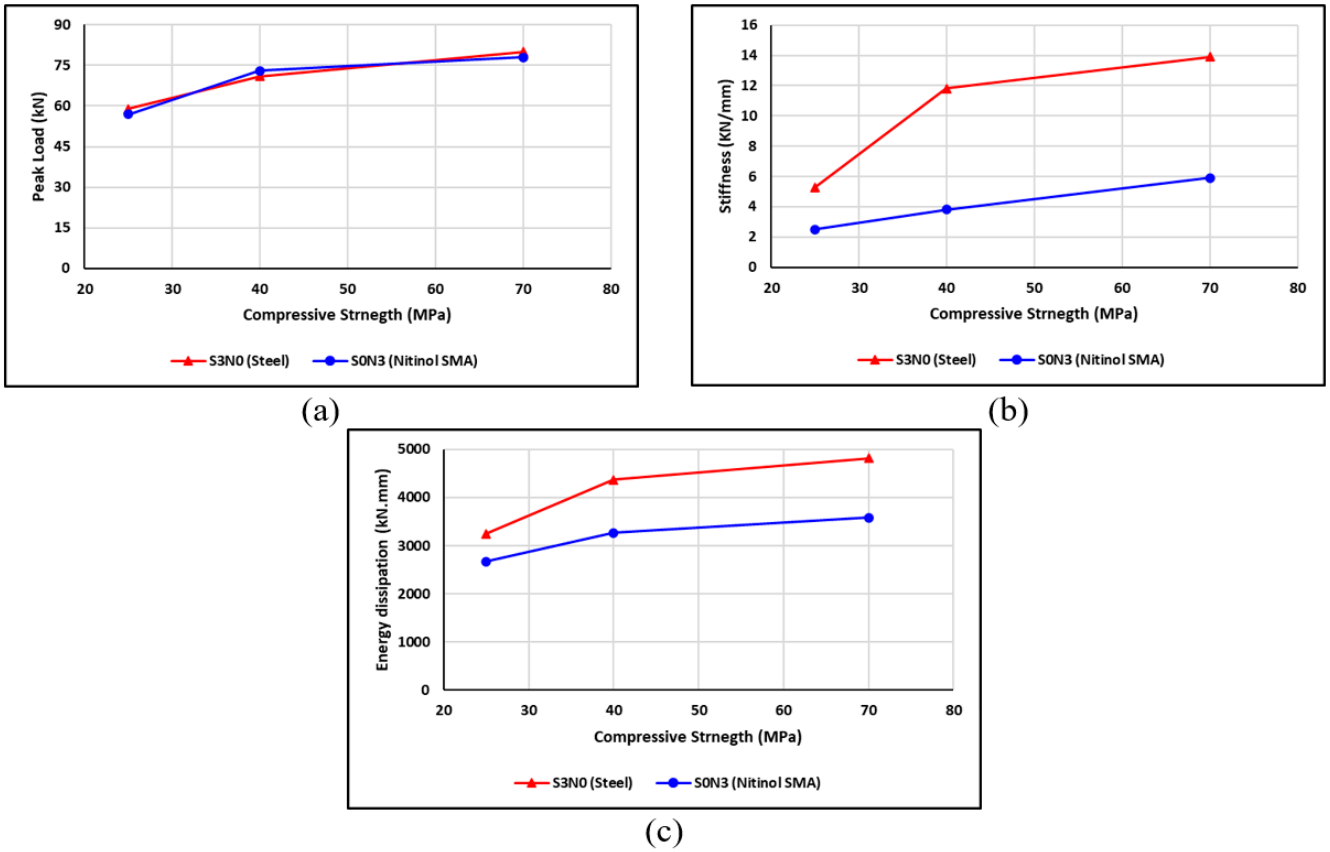

Figure 25. Effect of compressive strength of concrete of the BCJ on (**a**) load capacity, (**b**) stiffness, and (**c**) energy dissipation.

6.5. Effect of Axial Load

The effect of axial load applied at column end, on the behavior of RC joint, was investigated by considering three different levels of axial load, 15%, 30%, and 60% of column load capacity. The specimens investigated include BCJ reinforced with steel rebars: C25-A15-S3N0, C25-A30-S3N0 and C25-A60-S3N0; and BCJ reinforced with SMA bars: C25-A15-S0N3, C25-A30-S0N3 and C25-A60-S0N3. Keeping all other parameters constant, the compressive strength of concrete used for studying the effect of axial load was 25 MPa. The load–story drift ratio curves of BCJ reinforced with steel and SMA bars are shown in Figures 26 and 27. It is observed that raising the axial load from 0% to 60% of column load capacity enhanced the capacity of BCJ reinforced with steel and SMA bars by 24% or 14%, respectively, as seen in Figure 28a. The effect of axial load was more pronounced on the behavior of BCJ reinforced with steel rebars than that reinforced with SMA bars. The stiffness of BCJ reinforced with steel and SMA increased up to 40% and 32%, respectively, when the axial column load increased up to 60% of column capacity, as shown in Figure 28b. Moreover, the increase in the stiffness of the BCJ reinforced with steel was significant up to an axial load level of 15%, beyond which a steady state stiffness was observed, whereas the stiffness of the BCJ reinforced with SMA increased steadily as the axial load was increased. The effect of axial load level on the dissipated energy was higher than its effect on the load capacity or the stiffness of the BCJ. The energy dissipated increased by 26%, 28% and 43% for the BCJ reinforced with steel bars when the axial load level was increased from 0% to 15%, and 30% to 60%, respectively, as shown in Figure 28c. Almost, similar behavior was noticed for the BCJ reinforced with SMA bars.

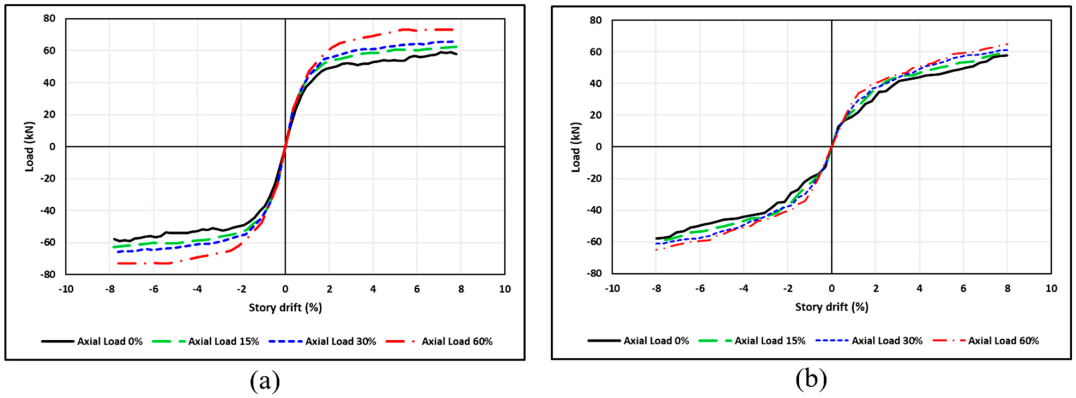

Figure 26. Numerical beam tip-load versus story drift envelopes of the BCJ (**a**) C25-A0-S3N0, C25-A15-S3N0, C25-A30-S3N0 and C25-A60-S3N0 specimens; (**b**) C25-A0-S0N3, C25-A15-S0N3, C25-A30-S0N3 and C25-A60-S0N3 specimens.

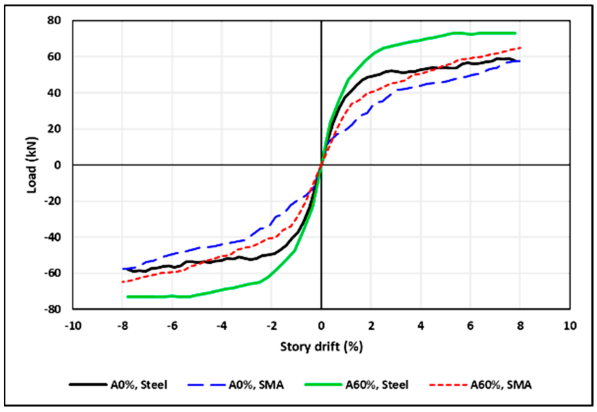

Figure 27. Effect of axial load level on the load capacity of the BCJ.

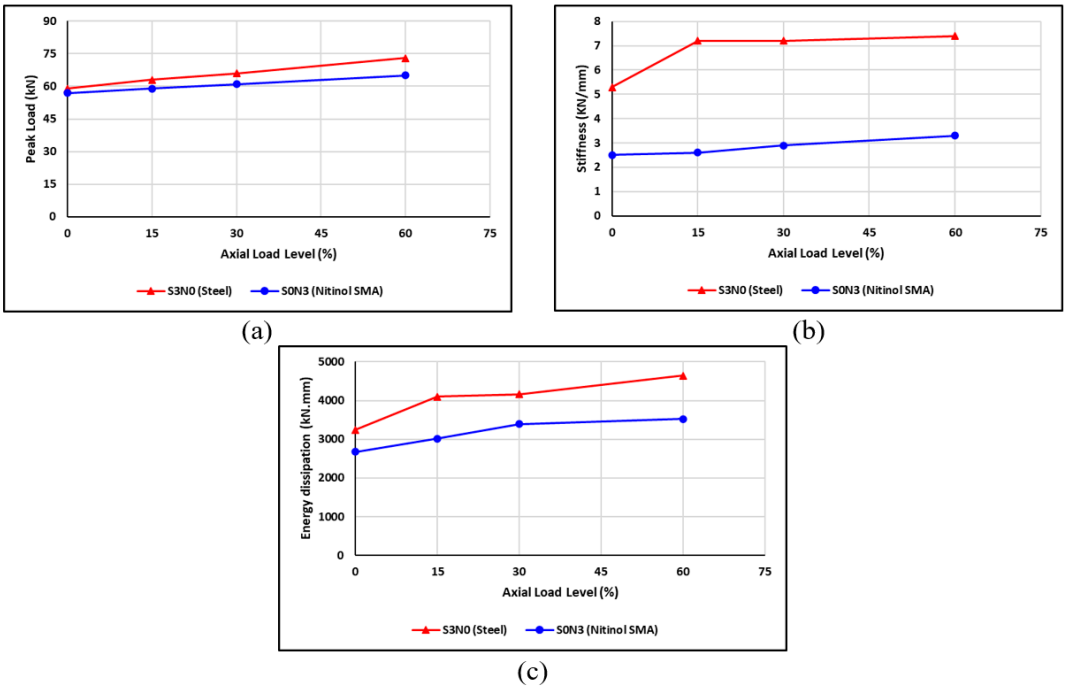

Figure 28. Effect of axial load level of the BCJ on (**a**) load capacity, (**b**) stiffness, and (**c**) energy dissipation.

7. Discussion of Beam–Column Joints Response

The numerical results obtained from the current parametric study are summarized in Table 7. The effects of the key parameters investigated on the response of RC-BCJ can best be explained and understood by normalizing the load capacity, stiffness, and energy dissipation of control specimens C25-A0-S3N0 and C25-A0-S0N3 and making it equal to 1, as shown in the subsequent sections.

Table 7. Numerical test results of the BCJ investigated.

#	Parameter	Specimen ID	Peak Load (kN)	Stiffness (kN/mm)	Energy Dissipated (kN/mm)
1	Control	C25-A0-S3N0	59	5.3	3247
2		C25-A0-S0N3	57	2.5	2677
3	SMA–steel reinforcement	C25-A0-S1N2	57	4.8	2956
4		C25-A0-S2N1	58	5.2	3194
5	Length of SMA	C25-A0-S0N3-L180	58	4.6	2699
6		C25-A0-S0N3-L540	57	2.5	2673
7	Elastic modulus of SMA	C25-A0-S0N3-E57	55	3.7	3011
8		C25-A0-S0N3-E82	56	4.0	3043
9	Concrete Compressive Strength	C40-A0-S3N0	71	11.8	4375
10		C70-A0-S3N0	80	13.9	4818
11		C40-A0-S0N3	73	3.8	3269
12		C70-A0-S0N3	78	5.9	3585
13	Axial load level	C25-A15-S3N0	63	7.2	4103
14		C25-A30-S3N0	66	7.2	4167
15		C25-A60-S3N0	73	7.4	4641
16		C25-A15-S0N3	59	2.6	3014
17		C25-A30-S0N3	61	2.9	3394
18		C25-A60-S0N3	65	3.3	3522

7.1. Load Capacity of Beam–Column Joints

The normalized peak load of the RC-BCJ reinforced with SMA is presented in Figure 29. The BCJ specimen with: no axial column load (A0), concrete strength of 25 MPa (C25), three SMA bars (S0N3) with elastic modulus of 32 GPa (E32), length of SMA 360 mm (L360), was considered as the control specimen by normalizing the peak load and making it equal to 1. The effects of the various parameters investigated on the peak load are also presented in Figure 29. It can be observed that increasing concrete strength from 25 to 40 MPa (60% increase) resulted in improving the peak load by 28%, whereas the increase in axial load from 0% to 60% increased the peak load by 14%. The combined effect of high concrete strength and SMA bars could boost the role of SMA in enhancing the BCJ response. However, the elastic modulus and/or the length of SMA had no effect on the load capacity of the BCJ.

Figure 30 shows the normalized peak load of BCJ reinforced with steel rebars. The BCJ specimen (C25-A0-S3N0) with no axial load, and concrete strength of 25 MPa was considered as the control specimen by normalizing the peak load normalized and making it equal to 1. It can be concluded that: increasing the concrete strength from 25 to 40 MPa (60% increase) improved the peak load value by 20%, whereas the increase in axial load from 0% to 60%, increased the peak load by 24%. In general, the numerical analysis revealed that the use of the high-strength concrete could lead to further enhancement in the behavior of RC-BCJ compared to normal concrete joints. This is consistent with the results available in the literature [45–49]. Moreover, it is observed that changing the reinforcement type from steel to SMA caused no change in the peak load of the BCJ.

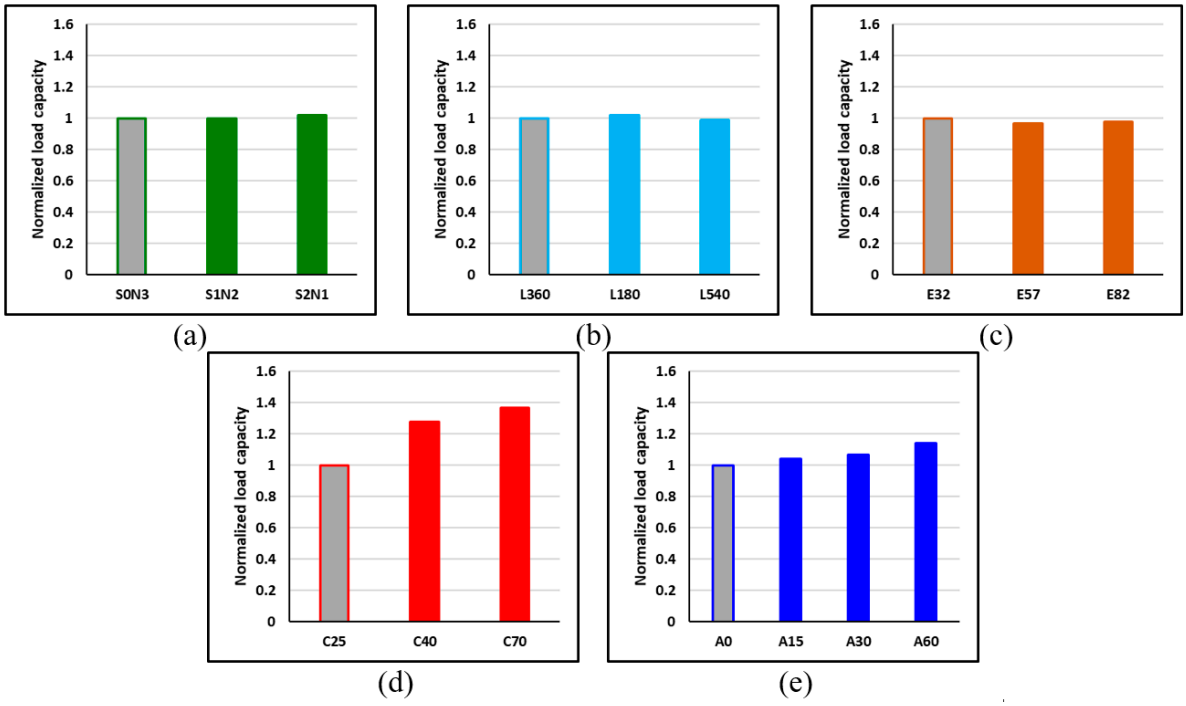

Figure 29. Comparisons of the effect of SMA on load capacity of the BCJ for the (**a**) SMA–steel reinforcement ratio, (**b**) lengths of SMA bars, (**c**) elastic modulus of SMA, (**d**) compressive strength of concrete, and (**e**) axial load level.

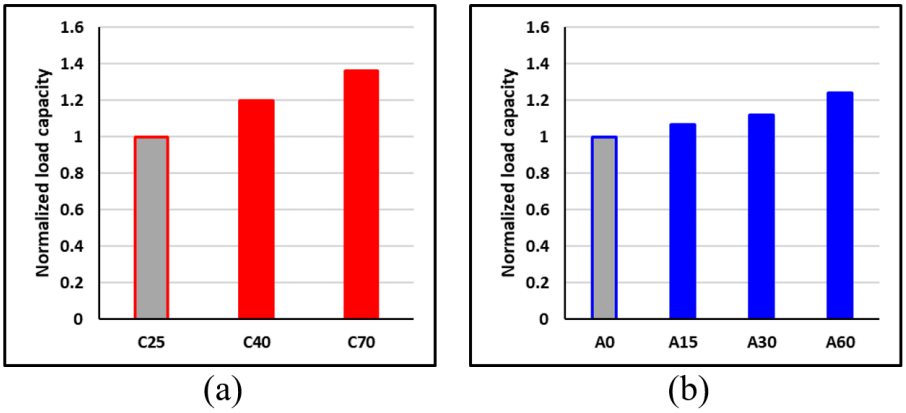

Figure 30. Comparisons of the effect of steel rebars on load capacity of BCJ for: (**a**) concrete strength; (**b**) axial load level.

7.2. Stiffness of Beam–Column Joints

The normalized stiffness of the BCJ reinforced with SMA is presented in Figure 31. The BCJ specimen with: concrete strength of 25 MPa (C25), 0% axial load level (A0), three SMA bars (S0N3), with elastic modulus of SMA of 32 GPa (E32), and length of SMA 360 mm (L360), was considered as the control specimen by normalizing the stiffness and making it equal to 1. The effects of the various parameters investigated on the stiffness are also presented in Figure 31. It can be observed that increasing concrete strength from 25 to 40 MPa (60% increase) or increasing axial load from 0% to 60% resulted in improving the stiffness by 52% or 32%, respectively. A further increase in elastic modulus of SMA from 32 to 57 GPa (78% increase) increased the stiffness of the BCJ by 48%. It can also be observed that the increase in stiffness due to combining SMA and steel reinforcement is more pronounced than the increase in stiffness due to increasing the elastic modulus of SMA only. Moreover, it was noticed that reducing the length of SMA from 360 to

180 mm increased the stiffness by 84%, while increasing the length from 360 to 540 mm had no effect on the stiffness value. It should be pointed out that adequate design length of SMA prevents the yielding of steel reinforcement and thus reduces the cracking and permanent deformations.

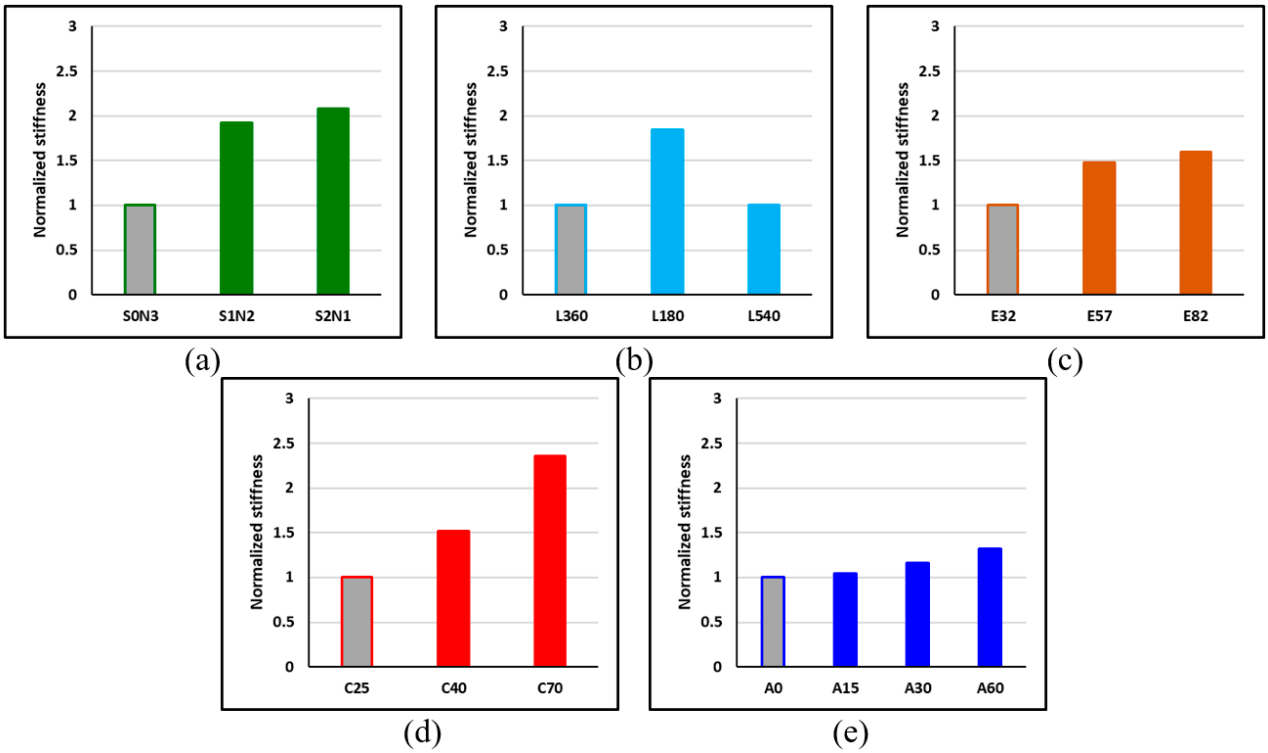

Figure 31. Comparisons of the effect of SMA on stiffness of the BCJ for the (**a**) SMA–steel reinforcement ratio, (**b**) lengths of SMA, (**c**) elastic modulus of elasticity of SMA, (**d**) compressive strength of concrete, and (**e**) axial load level.

The normalized stiffness of the joint specimen reinforced with steel only is shown in Figure 32. The BCJ specimen (C25-A0-S3N0) designed with: a concrete strength of 25 MPa, and 0% axial load, was considered as the control specimen by normalizing the stiffness and making it equal to 1. It can be observed that increasing the concrete strength from 25 to 40 MPa (60% increase) increased the stiffness by 123%, while increasing column axial load from 0% to 60% of the column capacity increased the stiffness by 40%. A further increase in concrete strength from 25 to 70 MPa increased the stiffness by 162%, while increasing the axial column load level up to 60% caused no more increase compared to 30% and 15% axial load levels.

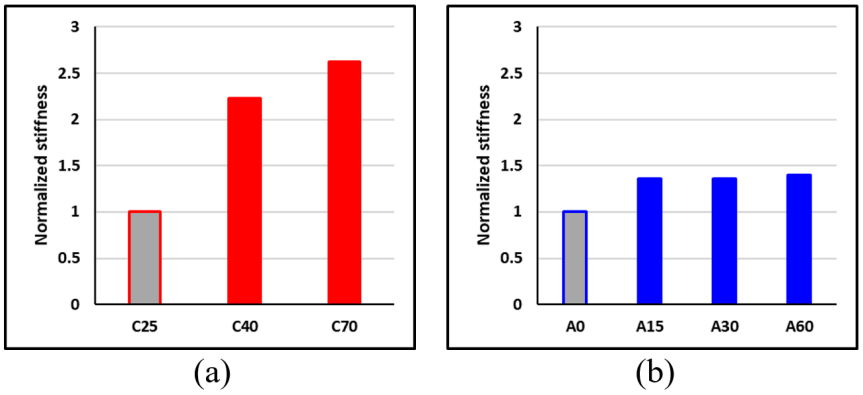

Figure 32. Comparisons of the effect of steel rebars on stiffness of BCJ for: (**a**) concrete strength; (**b**) axial load level.

7.3. Energy Dissipation of Beam Column Joints

The normalized energy dissipation of the BCJ reinforced with SMA is shown in Figure 33. The BCJ specimen with: concrete strength of 25 MPa (C25), 0% axial load level (A0), three SMA bars (S0N3), with elastic modulus of SMA of 32 GPa (E32), and length of SMA 360 mm (L360), was considered as the control specimen by normalizing the energy dissipated and making it equal to 1. The effects of the various parameters investigated on the energy dissipated are also presented in Figure 33. It can be observed that increasing the concrete strength from 25 to 40 MPa (60% increase) increased the energy dissipated by 22%, while the increase in axial load level from 0% to 60% increased the energy dissipated by 32%. A further increase in elastic modulus of SMA from 32 to 57 GPa (78% increase) increased the energy dissipated of the BCJ by 12%. It can also be observed that the increase in stiffness due to combining SMA and steel reinforcement had no effect on the energy dissipation of the joint. Moreover, the increase in the energy dissipated due to combining SMA and steel reinforcement is more pronounced than the increase in the energy dissipated due to increasing the elastic modulus of SMA only. It was also observed that varying the length of SMA from 360 to 180 or 540 mm had no effect on the energy dissipated. The normalized energy dissipated by BCJ reinforced with steel is shown in Figure 34. It can be noticed that increasing the concrete strength by 60% or increasing the level of axial load by 60% resulted in enhancing the energy dissipated by 35% and 43%, respectively.

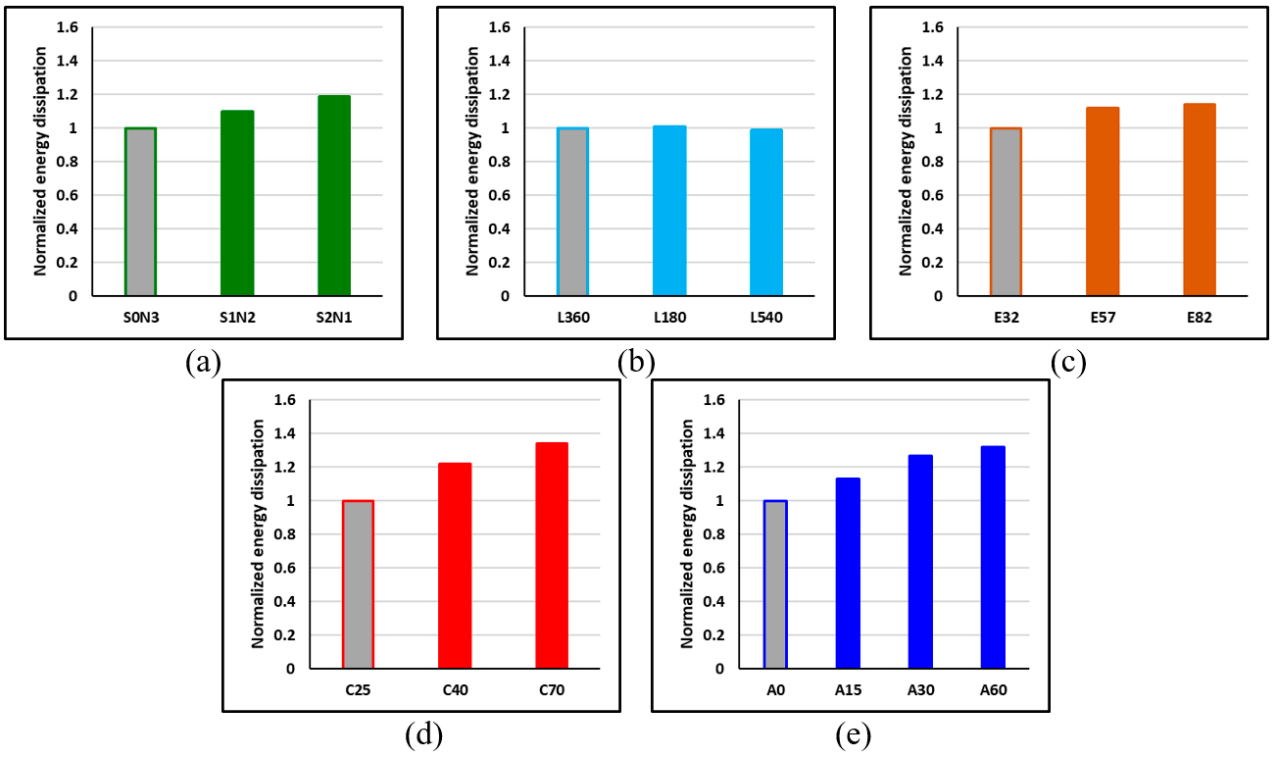

Figure 33. Comparisons of the effect of SMA on energy dissipation of the BCJ for the (**a**) SMA–steel reinforcement ratio, (**b**) lengths of SMA, (**c**) elastic modulus of SMA, (**d**) compressive strength of concrete, and (**e**) axial load level.

The interaction among some of the important parameters investigated is shown in Figure 35. The figure demonstrates the interaction between concrete strength and length of SMA bars in terms of peak load, stiffness, and energy dissipation. It is observed that the increase in concrete strength causes a significant increase in load capacity and energy dissipation of the RC joints, while the increase in the length of SMA bars has a slight effect on the load capacity and energy dissipation values. Moreover, Figure 35 illustrates that the increase in the length of SMA bars resulted in a significant reduction in the stiffness of the RC joint because of the low value of the elastic modulus of SMA compared to that of steel.

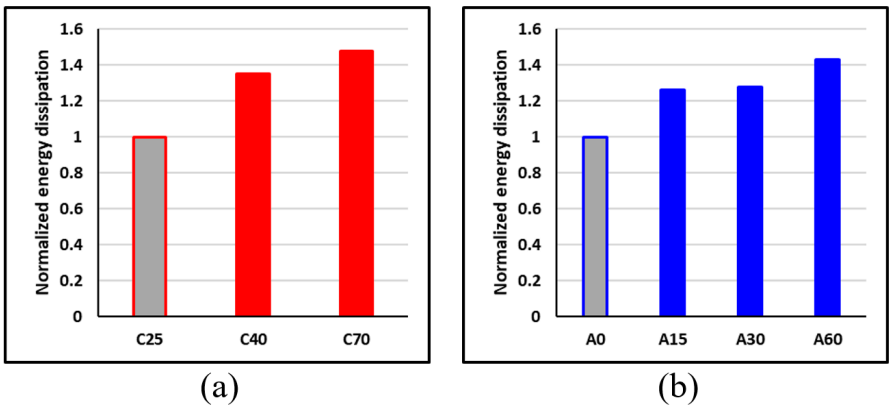

Figure 34. Comparisons of the effect of steel rebars on the energy dissipation of BCJ for: (**a**) concrete strength; (**b**) axial load level.

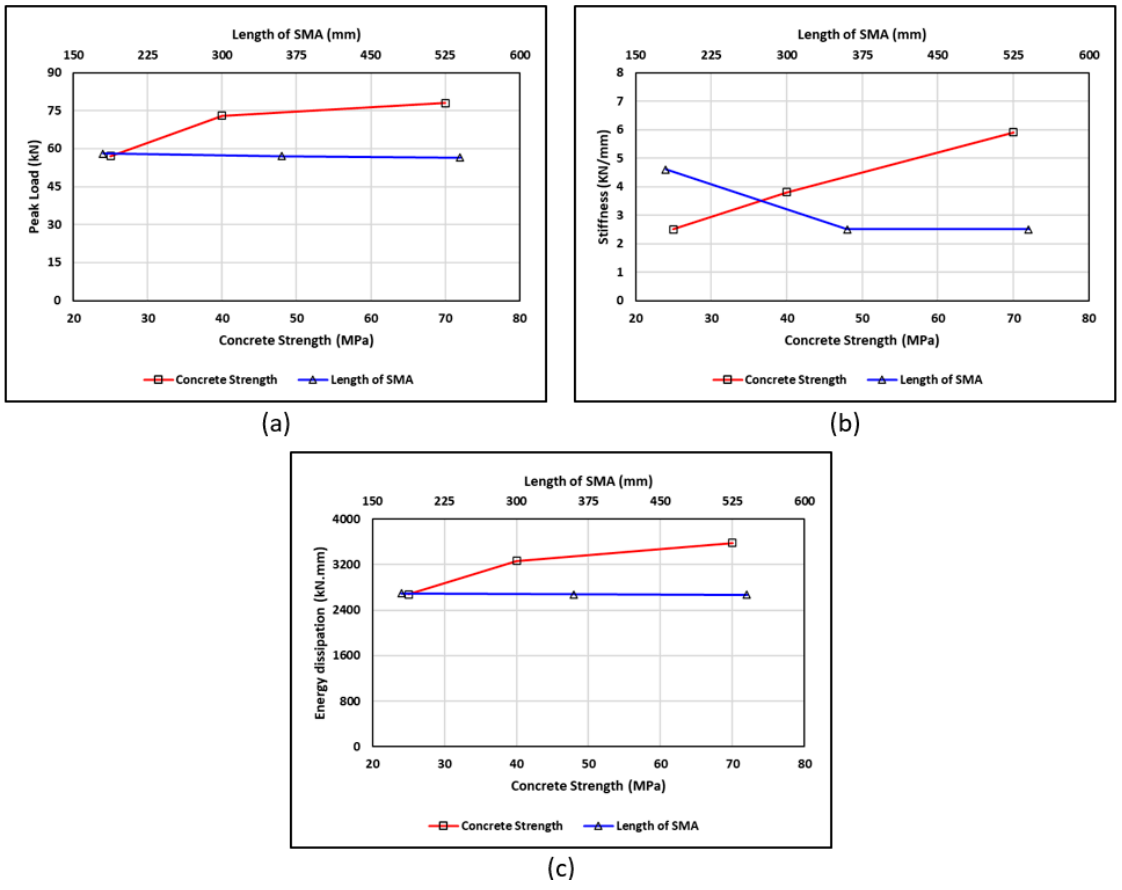

Figure 35. Comparisons of the effect of the length of SMA and concrete strength parameters on the BCJ for: (**a**) peak load, (**b**) stiffness, and (**c**) energy dissipation.

8. Conclusions

A numerical investigation through finite element analysis was carried out for evaluating the performance of RC-BCJ reinforced with SMA in conjunction with steel rebars. Based on the FE simulations presented, the following conclusions could be drawn:

- A non-linear finite element model was proposed using ABAQUS for evaluating the seismic performance RC-BCJ. The validated model could be considered as an effective design tool for predicting the performance of RC-BCJ under monotonic lateral loading.
- The model was capable of predicting the optimum length of SMA bars sufficient for relocating the plastic hinge away from the face of the column along the beam. This will

prevent yielding of steel rebars and thus eliminate the risk of permanent deformations in the joint region.

- The proposed hybrid system of SMA–steel reinforcement could be considered as an effective technique for improving the performance of the RC beam–column joints. This technique takes full advantage of the higher stiffness and higher energy dissipation provided by the steel, and the self-centering capability provided by SMA.
- The numerical results of this study could be considered as a useful reference for optimizing the performance of RC joints reinforced with SMA bars. Moreover, they are supposed to enrich the database on smart materials, and encourage the scientific community to explore their potential applications in various structures. This will definitely reduce the post-maintenance requirements of concrete structures built in active seismic zones.
- Among all the parameters investigated, the simulation results indicated that using high-strength concrete in the joint region was more effective in enhancing the efficiency of the joints.
- For specimens reinforced with SMA and steel rebars, the simulation results revealed the followings: (1) increasing the elastic modulus of SMA bars from 32 GPa to 82 GPa increased the stiffness of RC-BCJ up to 60%, (2) increasing the concrete strength from 25 up to 70 MPa, caused up to a 37% increase in load capacity, a 136% increase in stiffness, and a 34% increase in energy dissipation.
- Applying a constant axial load at the column end, up to 60% of the column capacity, increased lateral load capacity by 24%, stiffness by 40% and energy dissipation by 43%.
- The current investigation could be extended further to analyze the behavior of some other structural members such as column-footing connections, bridges piers, and beams. It is worth mentioning that further investigation on the coupler connecting the steel reinforcement with SMA bars, and the bond performance of SMA bars embedded in concrete, would be essential for the safe design of concrete structures reinforced with SMA.

Author Contributions: Conceptualization, M.M.H., M.J.A. and A.S.A.; methodology, M.M.H., M.J.A. and A.S.A.; software, M.M.H.; validation, M.M.H.; formal analysis, M.M.H., M.J.A. and A.S.A.; investigation, M.M.H., M.J.A. and A.S.A.; resources, A.S.A.; data curation, M.M.H., M.J.A. and A.S.A.; writing—original draft preparation, M.M.H. and M.J.A.; writing—review and editing, M.J.A. and A.S.A.; visualization, M.M.H.; supervision, M.J.A. and A.S.A.; project administration, M.J.A. and A.S.A.; funding acquisition, A.S.A. All authors have read and agreed to the published version of the manuscript.

Funding: This research was funded by Deputyship for Research and Innovation, Ministry of Education in Saudi Arabia through the project no. (IFKSUOR3-581-1).

Data Availability Statement: The datasets generated and/or analyzed during the current study are available from the corresponding author upon reasonable request.

Acknowledgments: The authors extend their appreciation to the Deputyship for Research and Innovation, Ministry of Education in Saudi Arabia for funding this research work through the project no. (IFKSUOR3-581-1).

Conflicts of Interest: The authors declare no conflict of interest.

References

1. Kawashima, K.; MacRae, G.A.; Hoshikuma, J.-I.; Nagaya, K. Residual Displacement Response Spectrum. *J. Struct. Eng.* **1998**, *124*, 523–530. [CrossRef]
2. Bazzurro, P.; Cornell, C.A.; Menun, C.A.; Motahari, M. Guidelines for seismic assessment of damaged buildings. In Proceedings of the 13th World Conference on Earthquake Engineering, Vancouver, BC, Canada, 1–6 August 2004.
3. Luco, N.; Bazzurro, P.; Cornell, C.A. Dynamic versus static computation of the residual capacity of a mainshock damaged building to withstand an aftershock. In Proceedings of the 13th World Conference on Earthquake Engineering, Vancouver, BC, Canada, 1–6 August 2004.

4. Cao, X.-Y.; Feng, D.-C.; Beer, M. Consistent seismic hazard and fragility analysis considering combined capacity-demand uncertainties via probability density evolution method. *Struct. Saf.* **2023**, *103*, 102330. [CrossRef]
5. Cao, X.-Y.; Feng, D.-C.; Li, Y. Assessment of various seismic fragility analysis approaches for structures excited by non-stationary stochastic ground motions. *Mech. Syst. Signal Process.* **2023**, *186*, 109838. [CrossRef]
6. Fang, C. SMAs for infrastructures in seismic zones: A critical review of latest trends and future needs. *J. Build. Eng.* **2022**, *57*, 104918. [CrossRef]
7. Mirzaey, E.; Shaikh, R.; Rasheed, M.; Ughade, A.; Khan, H.A.; Shaw, S.K. Shape memory alloy reinforcement for strengthening of RCC structures—A critical review. *Mater. Today Proc.* **2023**, *in press*. [CrossRef]
8. Alshannag, M.J.; Alqarni, A.S.; Higazey, M.M. Superelastic Nickel–Titanium (NiTi)-Based Smart Alloys for Enhancing the Performance of Concrete Structures. *Materials* **2023**, *16*, 4333. [CrossRef]
9. Suhail, R.; Amato, G.; Alam, M.S.; Broderick, B.; Grimes, M.; McCrum, D. Seismic Retrofitting of Nonseismically Detailed Exterior Reinforced Concrete Beam-Column Joint by Active Confinement Using Shape Memory Alloy Wires. *J. Struct. Eng.* **2023**, *149*, 04023003. [CrossRef]
10. Qian, H.; Wu, P.; Ren, Z.; Chen, G.; Shi, Y. Pseudo-static tests of reinforced concrete pier columns confined with pre-tensioned superelastic shape memory alloy wires. *Eng. Struct.* **2023**, *280*, 115680. [CrossRef]
11. Zareie, S.; Issa, A.S.; Seethaler, R.J.; Zabihollah, A. Recent advances in the applications of shape memory alloys in civil infrastructures: A review. *Structures* **2020**, *27*, 1535–1550. [CrossRef]
12. Ozbulut, O.E.; Hurlebaus, S.; Desroches, R. Seismic Response Control Using Shape Memory Alloys: A Review. *J. Intell. Mater. Syst. Struct.* **2011**, *22*, 1531–1549. [CrossRef]
13. Saadat, S.; Salichs, J.; Noori, M.; Hou, Z.; Davoodi, H.; Bar-On, I.; Suzuki, Y.; Masuda, A. An overview of vibration and seismic applications of NiTi shape memory alloy. *Smart Mater. Struct.* **2002**, *11*, 218–229. [CrossRef]
14. Desroches, R.; Smith, B. Shape Memory Alloys in Seismic Resistant Design and Retrofit: A Critical Review of Their Potential and Limitations. *J. Earthq. Eng.* **2004**, *8*, 415–429. [CrossRef]
15. Wilson, J.C.; Wesolowsky, M.J. Shape Memory Alloys for Seismic Response Modification: A State-of-the-Art Review. *Earthq. Spectra* **2005**, *21*, 569–601. [CrossRef]
16. Song, G.; Ma, N.; Li, H.-N. Applications of shape memory alloys in civil structures. *Eng. Struct.* **2006**, *28*, 1266–1274. [CrossRef]
17. Li, B.; Leong, C.L. Experimental and Numerical Investigations of the Seismic Behavior of High-Strength Concrete Beam-Column Joints with Column Axial Load. *J. Struct. Eng.* **2015**, *141*, 9. [CrossRef]
18. *DIANA*, version 7; (Computer Software); TNO Building and Construction Research: Delft, The Netherlands.
19. Youssef, M.A.; Alam, M.S.; Nehdi, M. Experimental Investigation on the Seismic Behavior of Beam-Column Joints Reinforced with Superelastic Shape Memory Alloys. *J. Earthq. Eng.* **2008**, *12*, 1205–1222. [CrossRef]
20. Halahla, A.; Abu Tahnat, Y.; Almasri, A.; Voyiadjis, G. The Effect of Shape Memory Alloys on theDuctility of Exterior Reinforced Concrete Beam-Column Joints Using the Damage Plasticity Model. *Eng. Struct.* **2019**, *200*, 109676. [CrossRef]
21. *ABAQUS*, Analysis User's Manual Version 2020; Dassault Systems Simulation Corp.: Providence, RI, USA, 2020.
22. Basim, S.; Hejazi, F.; Rashid, R.S.B.M. Embedded carbon fiber-reinforced polymer rod in reinforced concrete frame and ultra-high-performance concrete frame joints. *Int. J. Adv. Struct. Eng.* **2019**, *11*, 35–51. [CrossRef]
23. Shannag, M.J.; Abu-Farsakh, G.; Abu-Dyya, N. Modeling the cyclic response of fiber reinforced concrete joints. *Eng. Struct.* **2007**, *29*, 2960–2967. [CrossRef]
24. Cao, X.-Y.; Xiong, C.-Z.; Feng, D.-C.; Wu, G. Dynamic and probabilistic seismic performance assessment of precast prestressed reinforced concrete frames incorporating slab influence through three-dimensional spatial model. *Bull. Earthq. Eng.* **2022**, *20*, 6705–6739. [CrossRef]
25. Oudah, F.; El-Hacha, R. Innovative Self-Centering Concrete Beam-Column Connection Reinforced Using Shape Memory Alloy. *ACI Struct. J.* **2018**, *115*, 607–620. [CrossRef]
26. Miralami, M.; Esfahani, M.R.; Tavakkolizadeh, M. Strengthening of circular RC column-foundation connections with GFRP/SMA bars and CFRP wraps. *Compos. Part B Eng.* **2019**, *172*, 161–172. [CrossRef]
27. Ali, A.; Kim, D.; Cho, S.G. Modeling of nonlinear cyclic load behavior of i-shaped composite steel-concrete shear walls of nuclear power plants. *Nucl. Eng. Technol.* **2013**, *45*, 89–98. [CrossRef]
28. Grassl, P.; Jirásek, M. Damage-plastic model for concrete failure. *Int. J. Solids Struct.* **2006**, *43*, 7166–7196. [CrossRef]
29. Wan, S.; Loh, C.-H.; Peng, S.-Y. Experimental and theoretical study on softening and pinching effects of bridge column. *Soil Dyn. Earthq. Eng.* **2001**, *21*, 75–81. [CrossRef]
30. Abraik, E. Seismic performance of shape memory alloy reinforced concrete moment frames under sequential seismic hazard. *Structures* **2020**, *26*, 311–326. [CrossRef]
31. Alam, M.; Youssef, M.; Nehdi, M. Analytical prediction of the seismic behaviour of superelastic shape memory alloy reinforced concrete elements. *Eng. Struct.* **2008**, *30*, 3399–3411. [CrossRef]
32. Shrestha, B.; Hao, H. Parametric study of seismic performance of super-elastic shape memory alloy-reinforced bridge piers. *Struct. Infrastruct. Eng.* **2015**, *12*, 1076–1089. [CrossRef]
33. Xiang, N.; Chen, X.; Alam, M.S. Probabilistic seismic fragility and loss analysis of concrete bridge piers with superelastic shape memory alloy-steel coupled reinforcing bars. *Eng. Struct.* **2020**, *207*, 110229. [CrossRef]

34. Auricchio, F.; Taylor, R.L. Shape-memory alloys: Modelling and numerical simulations of the finite-strain superelastic behavior. *Comput. Methods Appl. Mech. Eng.* **1997**, *143*, 175–194. [CrossRef]
35. Auricchio, F.; Taylor, R.L.; Lubliner, J. Shape-memory alloys: Macromodelling and numerical simulations of the superelastic behavior. *Comput. Methods Appl. Mech. Eng.* **1997**, *146*, 281–312. [CrossRef]
36. Fugazza, D. Shape Memory Alloy Devices for Earthquake Engineering: Mechanical Properties, Constitutive Modelling and Numerical Simulations. Master's Thesis, University of Pavia, Pavia, Italy, 2003.
37. Park, H.; Eom, T. A Simplified Method for Estimating the Amount of Energy Dissipated by Flexure-Dominated Reinforced Concrete Members for Moderate Cyclic Deformations. *Earthq. Spectra* **2006**, *22*, 459–490. [CrossRef]
38. Eom, T.-S.; Park, H.-G. Evaluation of energy dissipation of slender reinforced concrete members and its applications. *Eng. Struct.* **2010**, *32*, 2884–2893. [CrossRef]
39. Hakuto, S.; Park, R.; Tanaka, H. Seismic Load Tests on Interior and Exterior BCJs with Substandard Reinforcing Details. *ACI Struct. J.* **2000**, *97*, 11–25.
40. Shin, M.; LaFave, J.M. Reinforced Concrete Beam-Column-Slab Connections Subjected to Earthquake Loading. *Mag. Concr. Res.* **2004**, *56*, 273–291. [CrossRef]
41. Shaw, S.K.; Sil, A. Experimental study on cyclic loading characteristics of fly ash as partial replacement of cement in beam-column joint. *Case Stud. Constr. Mater.* **2020**, *13*, e00362. [CrossRef]
42. Alshannag, M.; Alshmalani, M.; Alsaif, A.; Higazey, M. Flexural performance of high-strength lightweight concrete beams made with hybrid fibers. *Case Stud. Constr. Mater.* **2023**, *18*. [CrossRef]
43. Strnadel, B.; Ohashi, S.; Ohtsuka, H.; Ishihara, T.; Miyazaki, S. Cyclic Stress-Strain Characteristics of Ti-Ni and Ti-Ni-Cu Shape Memory Alloys. *Mater. Sci. Eng. A* **1995**, *202*, 148–156. [CrossRef]
44. Raza, S.; Shafei, B.; Saiidi, M.S.; Motavalli, M.; Shahverdi, M. Shape memory alloy reinforcement for strengthening and self-centering of concrete structures—State of the art. *Constr. Build. Mater.* **2022**, *324*, 126628. [CrossRef]
45. Janke, L. Applications of shape memory alloys in civil engineering structures—Overview, limits and new ideas. *Mater. Struct.* **2005**, *38*, 578–592. [CrossRef]
46. Shannag, M.J.; Abu-Dyya, N.; Abu-Farsakh, G. Lateral load response of high performance fiber reinforced concrete beam–column joints. *Constr. Build. Mater.* **2005**, *19*, 500–508. [CrossRef]
47. Shannag, M.J.; Alhassan, M.A. Seismic Upgrade of Interior Beam-Column Subassemblages with High-Performance Fiber-Reinforced Concrete Jackets. *ACI Struct. J.* **2005**, *102*, 131–138. [CrossRef]
48. Shannag, M.J.; Higazey, M. Strengthening and Repair of a Precast Reinforced Concrete Residential Building. *Civ. Eng. J.* **2020**, *6*, 2457–2473. [CrossRef]
49. Alshannag, M.J.; Higazey, M. Condition assessment and renovation of an aged precast reinforced concrete multi-storey building. *IOP Conf. Series: Earth Environ. Sci.* **2022**, *1026*, 012016. [CrossRef]